Article

Highly stable N-doped carbon-supported Pd-based catalysts prepared from biomass waste for H2 production from formic acid

Jessica Chaparro-Garnica, Miriam Navlani-García, David Salinas-Torres, Emilia Morallon, and Diego Cazorla-Amoros

ACS Sustainable Chem. Eng., **Just Accepted Manuscript** • DOI: 10.1021/acssuschemeng.0c05906 • Publication Date (Web): 08 Sep 2020

Highly stable N-doped carbon-supported Pd-based catalysts prepared from biomass waste for H_2 production from formic acid

Jessica Chaparro-Garnica[†], Miriam Navlani-García[†], David Salinas-Torres[‡], Emilia Morallón[‡], Diego Cazorla-Amorós[†]*

[†]Departamento de Química Inorgánica e Instituto de Materiales, Universidad de Alicante, Apartado 99, Alicante, E-03080, España

[‡]Departamento de Química Física e Instituto de Materiales, Universidad de Alicante, Apartado 99, Alicante, E-03080, España

***Corresponding Author*:** Diego Cazorla-Amorós, Departamento de Química Inorgánica e Instituto Universitario de Materiales, University of Alicante, P.O. Box 99, San Vicente del Raspeig, E-03080, Alicante, Spain. Phone number: +34965903946; Email: cazorla@ua.es

ABSTRACT. Excellent Pd supported on carbon catalysts for the dehydrogenation of formic acid were synthesized from a lignocellulosic biomass residue. The preparation of the carbon support consisted of a H_3PO_4-assisted hydrothermal carbonization (HTC) and activation of a hemp residue, and the subsequent nitrogen functionalization. It was observed that the presence of nitrogen groups influenced both the size and the electronic properties of the Pd nanoparticles, which ultimately affected their catalytic properties. Furthermore, the catalytic performance also depended on the synthesis conditions used in the preparation of the catalysts (i.e. reduction of the Pd nanoparticles with $NaBH_4$ prior to the catalytic test or *in-situ* reduction). The best-performance catalysts (Pd/-N-HTC (n.r.)), which was prepared by *in-situ* reduction of the nanoparticles, displayed a remarkable catalytic activity with a very high TOF number of 8365 h^{-1} (TOF value calculated for the 2nd catalytic run and expressed per surface Pd atom) and outstanding stability during 6 consecutive reaction cycles, although the initial activity is maintained for 12 cycles. The catalytic system studied is among the most stable ever reported Pd-based heterogeneous catalyst for the dehydrogenation of formic acid.

KEYWORDS. Biomass upgrading, N-doped carbon, formic acid, hydrogen production, palladium nanoparticles

Introduction

A primary challenge facing society nowadays is the production of energy in a green and efficient way. Most of the energy used in all sectors comes from fossil fuels (coal, oil, and natural gas), which are intrinsically linked to the emission of CO_2 and the subsequent harmful effects for humans and the environment. Since more than 75 % of the greenhouse gasses emission from human activities is related to the production of energy, finding alternative energy sources and use has become mandatory.[1–3] Biomass is a renewable natural carbon resource, which is considered an auspicious alternative to fossil fuels, as well as a platform for the synthesis of high value-added products. [4] Biomass can be used as solid fuels and it can also be converted into gas and liquid fuels and different platform chemicals.[4–8] The great possibilities of biomass utilization have led to the concept of "biorefinery", that integrates conversion processes to produce fuels, power, heat, and value-added chemicals by targeting the utilization of all carbon atoms of the resource.[4]

Formic acid has recently received great attention as an interesting energy carrier that can be derived from biomass feedstocks. It can be obtained from hemicellulose, cellulose, lignin, and vegetable oils components using acid hydrolysis, wet oxidation, and catalytic oxidation processes.[9,10]

As for the role of formic acid in the energy scenario, it can be either used as a fuel in direct formic acid fuel cells (DFAFCs)[11] or in the production of hydrogen, as a liquid organic hydrogen carrier molecule.[12] Moreover, formic acid can be also used to produce other fuels and fuel intermediates, such as γ-valerolactone and methanol.[9,13,14] Among those options, its advantages as hydrogen carrier molecule have been widely studied.[15–20] Formic acid is the simplest carboxylic acid (HCOOH) and it has a volumetric hydrogen capacity of ~53.4 g L^{-1}, equivalent to 4.4 wt. % of H_2, which is very close to the value set by the US Department of Energy for efficient H_2 storage

substances for light-duty fuel cell vehicles.[10,21,22] The dehydrogenation of formic acid into H_2 can take place under mild conditions provided that suitable metal catalysts are used. Among those investigated options, heterogeneous Pd-based catalysts have been reported to be the most promising option; however, most of the systems lack of stability under reaction conditions, which is one of the most important drawbacks.[16,23–25] Carbon materials are the preferred supports to develop efficient catalysts to boost the generation of hydrogen from formic acid, offering large surface area and surface functional groups that serve as the anchoring points of metal nanoparticles. In particular, nitrogen-doped carbon materials have been shown to result in high-performing catalysts, which has been attributed to both the modification of Pd electronic properties and the direct participation of the nitrogen groups in the dehydrogenation of formic acid.[26–29]

Biomass valorization towards the development of efficient carbon-based materials for energy and environmental applications is the focus of great interest.[30–38] In this work, we aim at emphasizing the potential of biomass upgrading by developing a N-doped biomass-derived activated carbon that was further used as support of catalysts applied in the production of hydrogen from formic acid, which, as previously mentioned, is considered a promising biomass-derived hydrogen source, thus emphasizing the sustainable approach herein addressed. A hemp residue was used as the starting material for the synthesis of low cost and high yield activated carbon by H_3PO_4-assisted hydrothermal carbonization (HTC) and further heat-treatment, which was subsequently doped with nitrogen through an organic reaction under mild conditions. The resulting N-doped carbon was loaded with Pd nanoparticles to obtain Pd-based catalysts, which displayed excellent performance and outstanding stability even after 6 consecutive catalytic cycles of 30 min at 75 ºC, thus circumventing one of the main limitations of most catalysts used for this application. Additionally, the best-performance catalyst preserved its initial activity (in terms of TOF value)

even after 12 consecutive reaction cycles, which makes this catalyst one of the most stable heterogeneous catalyst ever reported for the dehydrogenation of formic acid. The present study highlights the importance of biomass valorization towards the development of efficient carbon-based materials for the production of hydrogen, which is a central issue in the sustainable energy and environmental scenario.

Experimental

Preparation of biomass-derived activated carbon and its N-doped counterpart

The biomass-derived activated carbon was obtained from hemp residue (HR) by H_3PO_4-assisted HTC.[32] The synthesis was performed by mixing 1 g of HR with a low-concentrated aqueous solution of H_3PO_4 (25 wt. %) in a 50 mL Teflon-lined stainless-steel autoclave (weight ratio of H_3PO_4/HR equal to 1). The autoclave was heated at 200 °C for 24 h. The resulting hydrochar was heated at 450 ºC for 2 h in N_2 atmosphere (50 mL min^{-1}). The obtained activated carbon was washed with distilled water at 65 °C and was dried at 110 °C overnight. The yield of the process was ~ 40 wt. % from the hemp residue precursor. The resulting activated carbon was denoted as HTC. The surface chemistry of the activated carbon was modified by introducing nitrogen groups (N-HTC) through an organic reaction under mild conditions, following the procedure described below: 45 mL of 2 M NH_4NO_3/DMF solution was prepared in a round bottom flask, then 300 mg of activated carbon was added under constant stirring. Subsequently, 45 mL of pyridine was added dropwise at room temperature (ratio of 1 g of activated carbon/300 mL solution). The mixture was kept stirring and its temperature was increased up to 70 °C and it was kept for 65 h. The N-doped activated carbon obtained was washed with abundant water and ethanol, filtered and dried at 110 °C for 12 h.[39] The as-synthesized support was denoted as N-HTC.

Preparation of Pd-based catalysts

Both HTC and N-HTC were used as supports to prepare Pd-based catalysts by a conventional wet impregnation method.[26] For that, 0.5 g of carbon support was dispersed in acetone (50 mL) and a specific volume of a 0.01 M $Pd(OAc)_2$ solution was added to achieve a final metal content of 1 wt. % and the mixture was stirred for 4 h at room temperature. After that, the metal precursor was reduced with $NaBH_4$ by stirring 1 h more, and the solvent was removed. Finally, the catalysts were washed with distilled water and dried at 60 ºC overnight. The resulting catalysts were denoted as Pd/HTC and Pd/N-HTC. An additional catalyst was prepared using N-HTC as support in which the reduction step was suppressed (Pd/N-HTC (n.r.)). A reference catalyst comprised of Pd nanoparticles supported on graphitic carbon nitride (g-C_3N_4) was also synthesized as reference material. For that, g-C_3N_4 was previously obtained from dicyandiamide by thermal decomposition at 520 ºC for 4 h (heating rate of 5 ºC min^{-1}) in air, and the resulting solid was impregnated with the Pd precursor to achieve Pd/g-C_3N_4 by following the same experimental protocol as that used in the preparation of Pd/N-HTC. The Pd content was 0.71 wt. %, the BET surface area was 13 m^2 g^{-1} and the Pd average particle size as determined from TEM was 6±2 nm.

Characterization

The porous texture of HTC, N-HTC, and Pd-based catalysts was determined by physical adsorption-desorption of N_2 at -196 °C using an automatic adsorption system (Micromeritics ASAP 2020 analyzer). Prior to the analysis, samples were outgassed at 200 °C for 6 h to remove any possible adsorbed impurity. The apparent surface area and total micropore volume (V_{DR} N_2) were calculated applying the Brunauer-Emmett-Teller (BET) method and the Dubinin–Radushkevich (DR) equation to the N_2 adsorption isotherm at -196 ºC, respectively. Mesopore

volume was determined by calculating the difference between the volume of N_2 adsorbed at a relative pressure of 0.95 and the volume of micropores.[40] Pore size distributions were obtained from the 2D-NLDFT heterogeneous surface model using the SAIEUS software (available online at http://www.nldft.com/).[41]

The morphology of the catalysts was analyzed by Transmission Electron Microscopy (TEM) using a JEOL (JEM-2010) transmission electron microscope operating at 200 kV with a spatial resolution of 0.24 nm. Average nanoparticle size and size distribution were obtained after measuring ~ 100 nanoparticles in representative micrographs of each catalyst with the ImageJ software. The dispersion of Pd nanoparticle (D), defined as the number of Pd atoms on the surface of the sample divided by the total number of Pd atoms, was estimated by assuming spherical nanoparticle geometry.[42,43] Pd content was determined by Inductively Coupled Plasma-Optical Emission Spectroscopy (ICP-OES) with a Perkin-Elmer Optima 4300 system. X-ray photoelectron spectroscopy (XPS) analysis was performed in a VG-Microtech Multilab 3000 spectrometer equipped with a semispherical electron analyzer and a Mg Kα (hν=1253.6 eV) 300 W X-ray source. For the proper analysis, binding energies were referred to the C 1s line at 284.6 eV in all cases. N 1s and Pd 3d, characterized by two well separated spin-orbit coupling components (i.e. Pd $3d_{5/2}$ and Pd $3d_{3/2}$), were analyzed. The different species of N and Pd and their relative contents were calculated from the deconvoluted spectra. The deconvolution of the spectra was carried out by using Gaussian functions with 20% of Lorentzian component. FWHM of the peaks was kept between 1.6 and 1.8 eV and between 1.3 and 1.6 eV for N and Pd, respectively. A Shirley line was used for estimating the background signal.

Catalytic tests

The activity of the catalysts in the dehydrogenation of formic acid at 75 ºC was assessed by monitoring the gas evolution for 30 minutes. The catalytic runs were performed by placing 0.15 g of catalyst and the reaction mixture (an aqueous solution of formic acid and sodium formate with a molar ratio of 9 to 1, and a final concentration of 1 M) in a reactor, which was connected to a burette system. The stability of the catalysts was assessed by performing 6 consecutive reaction cycles and collecting the spent catalyst by filtration between two consecutive cycles. The stability of the best-performance catalyst was further evaluated by monitoring the reaction during 6 additional reaction cycles (12 consecutive reaction runs in total).

TOF values (h^{-1}) were calculated with the following equation (1):

$$\mathrm{TOF}\ (\mathrm{h}^{-1}) = \frac{\text{produced } H_2 \text{ (mole)}}{\text{Pd atoms (mole)} \times \text{time (h)}} \qquad (1)$$

where the produced H_2 (mole) is the mole of H_2 obtained after 4 min of reaction, and Pd atoms are determined from the Pd content obtained by ICP-OES analysis. Moreover, TOF values were also calculated on the basis of surface Pd atoms. For that, surface Pd atoms were calculated from the TEM average nanoparticle size (d_{TEM}) and Pd nanoparticle dispersion (D_{TEM}, which is defined as the percentage of atoms exposed on the surface of the nanoparticles), using the following expression (2):

$$\text{Surface Pd atoms} = \frac{\text{mole}_{Pd} * D_{TEM}}{100} \qquad (2)$$

The nanoparticle dispersion was estimated assuming spherical nanoparticle geometry and using the following equation (3):[42]

$$D_{TEM} = 10^{21}\frac{6M\rho_{site}}{\rho_{Pd}Nd_{TEM}} \qquad (3):$$

Where M (106.42 g/mol) is the atomic weight, ρ_{site} (12.7 atoms/nm^2) is the Pd surface site density, ρ_{Pd} (12.02 g/cm^3) is the metal density, N is Avogadro´s constant (6.022 * 10^{23} mol^{-1}), and d_{TEM} is the average diameter of the nanoparticles (nm).

Results and discussion

Catalysts characterization

Figure 1 depicts the N_2 adsorption-desorption isotherms (Figure 1(a)) and the pore size distribution profiles calculated by NLDFT (Figure 1(b)) of the carbon supports and Pd-based catalysts studied. As can be seen, all samples have a type I isotherm, according to the IUPAC classification,[40] which is characteristic of microporous solids. Pore size distribution profiles indicate that most of the pores are between 0.5 and 3 nm. Neither the introduction of nitrogen functional groups nor the incorporation of Pd nanoparticles modified considerably the porous texture of the starting activated carbon (HTC).

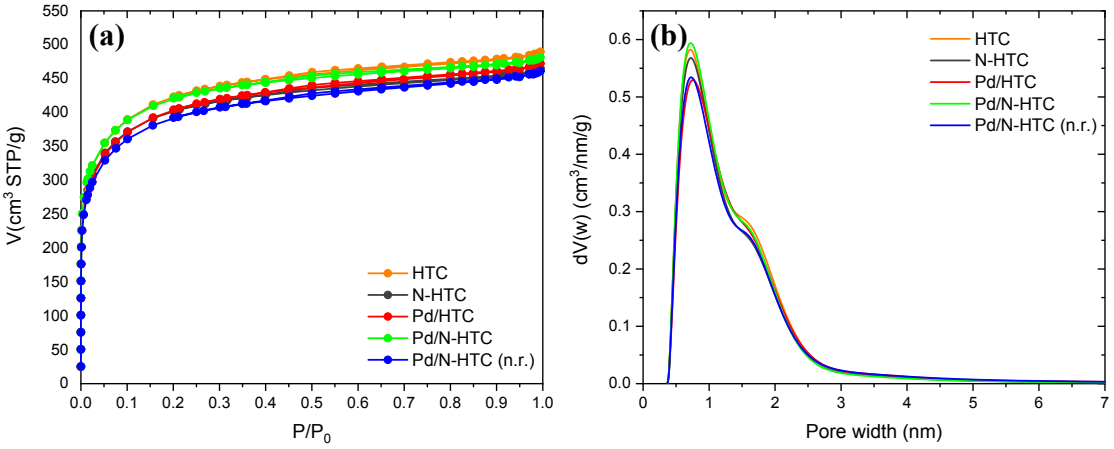

Figure 1. N_2 adsorption-desorption isotherms at -196 ºC of carbon supports and Pd-based catalysts (a) and their pore size distribution (b).

Table 1 includes the textural properties determined from the N_2 adsorption-desorption isotherms. The as-prepared activated carbon has an apparent surface area of 1535 $m^2\ g^{-1}$, which is mostly preserved after nitrogen functionalization and Pd loading. This is also the case for the micro and mesopore volumes.

Table 1. Porous texture characterization.

Sample	S_{BET} ($m^2\ g^{-1}$)	$V_{DR}\ N_2$ ($cm^3\ g^{-1}$)	$V_{meso}\ N_2$ ($cm^3\ g^{-1}$)
HTC	1535	0.64	0.10
N-HTC	1455	0.63	0.08
Pd/HTC	1465	0.63	0.08
Pd/N-HTC	1520	0.65	0.08
Pd/N-HTC (n.r.)	1420	0.60	0.10

As it was mentioned in the introduction section, most of the catalysts used in the dehydrogenation of formic acid lack of stability. Getting insight into the processes that lead to the deactivation of the catalysts under reaction conditions is crucial to achieving highly stable catalysts. Thus, the catalysts evaluated in the present study were characterized before and after performing 6 consecutive catalytic cycles and the results will be included in this section. As some reports have already addressed,[15,44,45] one of the main aspects to be checked is the nanoparticle size and distribution. In this study, such information was obtained by TEM analysis. Figure 2 includes representative TEM micrographs of the three Pd catalysts (both fresh and used) along with the histograms with the nanoparticle size distributions. Table 2 contains the average nanoparticle size and dispersion, as well as the Pd content determined by ICP analysis.

As can be seen in TEM images, Pd nanoparticles are well-dispersed and homogeneously distributed in all the as-prepared catalysts, which is due to the large surface area of the biomass-derived carbon support. The incorporation of nitrogen in the carbon support affects significantly the average Pd nanoparticle size. Pd/HTC catalyst has an average nanoparticle size of 3.9 nm and

relatively wide nanoparticle size distribution, whereas smaller average nanoparticle size and narrower size distribution were observed in the case of Pd/N-HTC prepared under the same experimental conditions (i.e. impregnation and subsequent reduction with $NaBH_4$). It should be noted that well-defined nanoparticles with an average particle size of 3.1 nm can also be observed in the catalyst Pd/N-HTC (n.r.), in which the reducing step with $NaBH_4$ was not carried out. As it will be later discussed, the electronic properties of the Pd nanoparticles present in Pd/N-HTC (n.r.) differ from those of Pd/N-HTC, since no Pd^0 was detected due to the suppression of the final reduction step. These results confirm the crucial role of nitrogen atoms in serving as anchorage sites for the metal precursor, thus resulting in smaller and well-distributed Pd nanoparticles.[46]

After performing 6 consecutive catalytic cycles (*vide infra*), Pd nanoparticles experienced an increase in the average size (and, thus a corresponding decrease in dispersion values). The size increase is of 72, 46, and 100 % for Pd/HTC_used, Pd/N-HTC_used, and Pd/N-HTC (n.r.)_used, respectively, as compared to their fresh catalyst counterparts. This observation indicates that both the incorporation of nitrogen in the catalyst and the previous reduction step affect the stability of the nanoparticles against sintering. On the one hand, the presence of nitrogen results in more stable nanoparticles when catalysts with pre-reduced nanoparticles are compared (Pd/HTC and Pd/N-HTC), once again confirming the ability of nitrogen functionalization in serving as metal anchoring sites and thus increasing the metal-support interaction.[26] On the other hand, the comparison of Pd/N-HTC and Pd/N-HTC (n.r.) suggests that pre-reduced nanoparticles display better stability against sintering than those *in-situ* reduced nanoparticles present in Pd/N-HTC (n.r.). Such observation might be related to the different nanoparticle reduction and growth kinetics in both Pd/N-HTC and Pd/N-HTC (n.r.) catalysts. In the case of Pd/N-HTC, Pd nanoparticles are reduced by $NaBH_4$ prior to the catalytic test, so that they might not be significantly affected by the

reducing atmosphere originated in the reaction medium caused by the formation of H_2 from formic acid. The pre-reduced Pd nanoparticles present in Pd/N-HTC might be stabilized by $NaBH_4$-derived species interacting with the surface of the nanoparticles, thus minimizing the sintering phenomena under reaction conditions.[47]

However, in Pd/N-HTC (n.r.), in which the metal species are not pre-reduced, most of the Pd nanoparticles are *in-situ* formed upon reduction with H_2 generated in the medium. The different reducing ability of $NaBH_4$ and H_2 and the different reduction conditions in both Pd/N-HTC and Pd/N-HTC (n.r.) catalysts might lead to different nanoparticle reduction and growth kinetics.[48,49] The relatively slow reduction rate for the *in-situ* reduction of Pd nanoparticles in Pd/N-HTC (n.r.) and the absence of species that may "protect" the nanoparticles growth, might be responsible for the larger nanoparticles increase and the wider particle size distribution observed in this catalyst.

ICP analysis confirmed that Pd was successfully loaded in all the fresh catalysts and that no significant metal leaching took place after performing 6 consecutive reaction runs. Such observation demonstrates the strong metal-support interaction between Pd nanoparticles and the biomass-derived carbon support synthesized in this study.

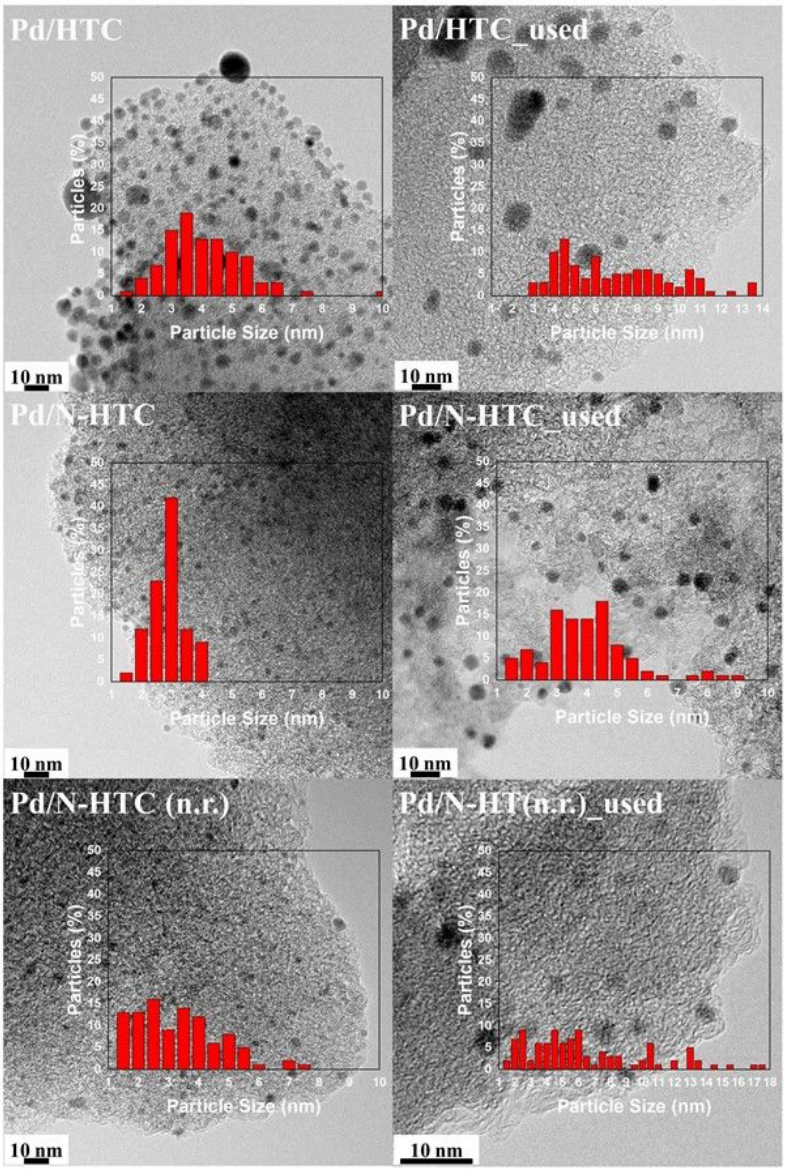

Figure 2. TEM micrographs and histograms with Pd nanoparticle size distributions for Pd/HTC, Pd/N-HTC, and Pd/N-HTC (n.r.).

Table 2. Results of TEM and ICP analysis.

Catalyst	d_{TEM} (nm)	D (%)	Pd loading wt. % (ICP)
Pd/HTC	3.9 ± 1.5	23.1	0.77
Pd/HTC_used	6.7 ± 2.6	12.9	0.74
Pd/N-HTC	2.6 ± 0.6	34.6	0.66
Pd/N-HTC_used	3.8 ± 1.6	23.7	0.63
Pd/N-HTC (n.r.)	3.1 ± 1.4	29.0	0.72
Pd/N-HTC (n.r.)_used	6.2 ± 3.8	14.5	0.68

Catalytic activity towards H_2 production

The results obtained from the catalytic tests are included in Figure 3. It should be mentioned that gas generation was not detected with the bare N-HTC support.

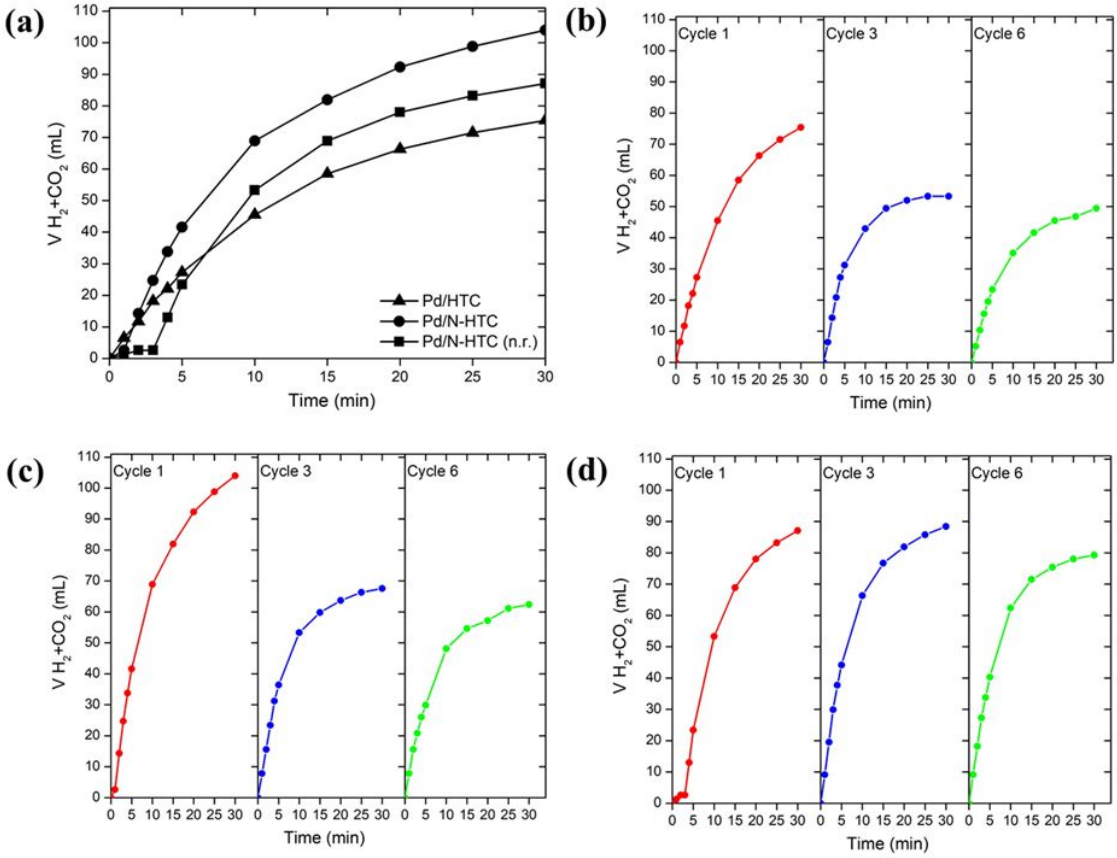

Figure 3. (a) Gas evolution profiles achieved in the 1st reaction cycle for Pd/HTC, Pd/N-HTC, and Pd/N-HTP (n.r.); (b) Gas evolution profiles of Pd/HTC in the 1st, 3rd and 6th cycle; (c) Gas

evolution profiles of Pd/N-HTC in the 1st, 3rd and 6th cycle; and (d) Gas evolution profiles of Pd/N-HTC (n.r.) in the 1st, 3rd and 6th cycle.

Figure 3 (a) depicts the gas evolution profiles achieved with the three catalysts in the first reaction cycle. Pd/HTC and Pd/N-HTC did not display induction time and the reaction proceeds smoothly, whereas with Pd/N-HTC (n.r.) an induction period of ~ 3 min was needed. This difference observed in the catalytic performance during the first reaction minutes can be ascribed to the different Pd species present in the catalysts. In this sense, Pd/HTC and Pd/N-HTC have pre-reduced Pd nanoparticles, so that the gas produced from the dehydrogenation of formic acid is rapidly accounted for the volume monitored. In the case of Pd/N-HTC (n.r.), not only the initial catalytic activity may be lower due to the lower amount of reduced Pd species, but also part of the H_2 generated during the first minutes of the first reaction cycle might be utilized in the reduction of Pd species. The differences in the electronic properties of Pd species in the three fresh catalysts can be clearly seen in Figure 4 (a) (*vide infra*).

The comparison of the gas evolution profiles achieved in the first reaction cycle also evidenced the positive role of nitrogen species. Even though the initial reaction rate observed in the Pd/HTC catalyst is comparable to that of Pd/N-HTC, the total volume of gas generated by N-containing catalysts is much larger than that produced by Pd/HTC (104, 87, and 75 mL of gas for Pd/N-HTC, Pd/N-HTC (n.r.), and Pd/HTC, respectively). Such positive effect of nitrogen in attaining good catalytic performance in the dehydrogenation of formic acid has been attributed to both the participation of nitrogen atoms in the reaction by interacting with formic acid molecules and increasing the local concentration close to the Pd active sites, and the role of nitrogen in modifying the electronic properties of Pd atoms. [26,50,51]

This latest effect can be checked by analyzing XPS results included in Figure 4.

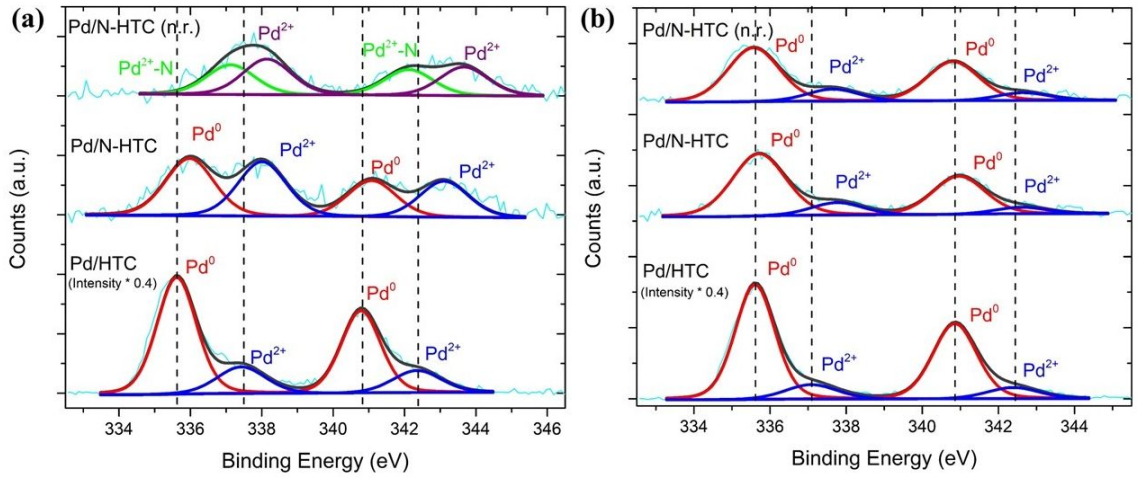

Figure 4. XPS Pd 3d of (a) fresh catalysts and (b) used catalysts (after 6 cycles).

XPS Pd spectrum contains two asymmetric doublets that can be assigned to $3d_{5/2}$ and $3d_{3/2}$ transitions, at lower and higher binding energies, respectively. As can be seen in Figure 4 (a), Pd/N-HTC showed a shift of ~ 0.4 eV towards higher binding energies in the Pd spectrum compared to that of Pd/HTC, which confirmed the modification of the electronic properties of Pd species by their interaction with the nitrogen functionalities incorporated in the catalysts.[24,52] Such positive shift of Pd spectra indicated the formation of electron-deficient Pd species and it is further corroborated by the relative proportion of Pd^0 and Pd^{2+} in Pd/HTC and Pd/N-HTC (77 and 23 % of Pd^0 and Pd^{2+}, and 51 and 49 % of Pd^0 and Pd^{2+}, in Pd/HTC and Pd/N-HTC, respectively), which indicated that the presence of nitrogen makes difficult the reduction of Pd^{2+} to Pd^0, even when a strong reducing agent (i.e. $NaBH_4$) is used,[53] so that Pd^{2+} species are stabilized by the nitrogen atoms incorporated in the support.[29] As for Pd/N-HTC (n.r.), only oxidized Pd species are present in the catalyst, since no pre-reduction step has been performed. Two possible contributions could also be distinguished in its spectrum, being both of them attributed to Pd^{2+} either in the free $Pd(OAc)_2$ (at 338.2 eV) or Pd^{2+} interacting with the N atoms of the support (at 337.1 eV).[54] The

XPS results of the used catalysts (Figure 4 (b)) indicated that both Pd^0 and Pd^{2+} are present in the nanoparticles, being Pd^0 the most abundant species in all of them.

As mentioned above, the significantly better performance observed in Figure 3 (a) for Pd/N-HTC compared to Pd/HTC catalysts may be related to the electronic properties of the Pd nanoparticles. Such aspect has been the focus of discrepancy in the literature, since there are authors who claim that electron-rich Pd species are the preferred active sites for the dehydrogenation of formic acid,[55] whereas the important role of electron-deficient Pd species has also been highlighted in other studies.[29] Recent studies have emphasized the role of both electron-rich and electron-deficient Pd species.[15,29,55]

Assuming the simplified reaction mechanism illustrated in Scheme 1,[55] the role of both electron-rich and electron-deficient Pd species could be understood. In that mechanism, the first reaction step consists in the adsorption of formate ion on the surface of Pd nanoparticles, which could be favoured by the presence of electron-deficient Pd species, whereas electron-rich Pd species favor the cleavage of the C-H bond of the adsorbed formate ion,[56] which is the second reaction step and has been reported to be the rate-limiting step in the overall catalytic reaction.[15,55] The reaction is finalized by release of H_2 and the regeneration of the catalyst.

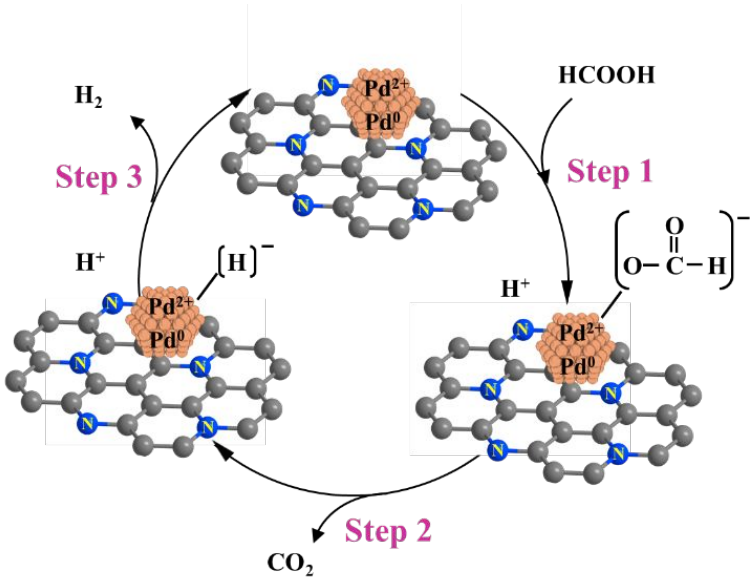

Scheme 1. Simplified reaction mechanism for the production of H_2 from formic acid.

Figure 5 includes the XPS N 1s spectra in the N-doped biomass-derived activated carbon support (N-HTC) and Pd/N-HTC catalysts.

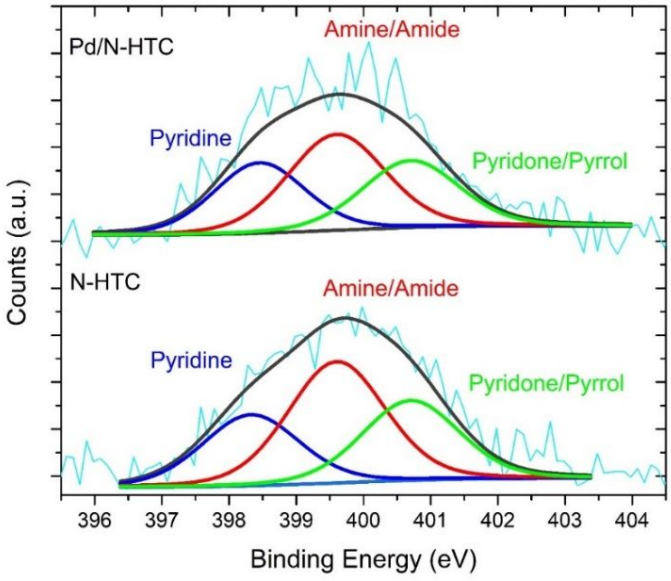

Figure 5. XPS N 1s spectra of N-HTC and N-HTC-supported Pd-based catalyst.

The XPS N1s spectrum of N-HTC shows three contributions, which can be attributed to the presence of pyridone/pyrrole, amine/amide, and pyridine groups, with a relative proportion of 26,

45, and 29 %, respectively.[57] As can be seen, the incorporation of Pd nanoparticles in Pd/N-HTC did not modify either the functional groups or their relative proportion. XPS analysis also indicated that the surface nitrogen content was ~ 1.8 at. %. This, together with the results of the catalytic performance, reveal that the positive role of the incorporation of nitrogen can be evidenced even with such low nitrogen content.

As for the reusability of the catalysts under reaction conditions, Figures 3 (b)-(d) depict the gas evolution profiles achieved in the 1st, 3rd, and 6th reaction cycle of Pd/HTC, Pd/N-HTC, and Pd/N-HTC (n.r.), respectively (the profiles recorded in the other cycles are not plotted for the sake of clarity). As can be seen, the three studied catalysts preserved relatively good catalytic activity even after 6 consecutive reaction cycles, after which they only lost 33, 40, and 9 % of the initial activity of Pd/HTC, Pd/N-HTC, and Pd/N-HTC (n.r.), respectively, in terms of total gas generated. Such aspect indicated that, even though better performance was achieved in the 1st reaction run for Pd/N-HTC than for Pd/N-HTC (n.r), the superior performance of Pd/N-HTC (n.r) is demonstrated by its outstanding stability under reaction conditions (it preserved 91 % of the initial activity, in terms of total volume of gas generated, after 6 consecutive cycles). In the light of the performance observed for Pd/N-HTC (n.r.), a first cycle is required in this case to attain the optimum working conditions of the catalyst, after which it shows extraordinary catalytic activity (TOF of 1214 h^{-1} and 8365 h^{-1} in the 2nd cycle, expressed on the basis of total Pd atoms and surface Pd atoms, respectively) and outstanding stability. None of the changes observed in the spent Pd/N-HTC (n.r.) catalyst compared to its fresh counterpart led to the deactivation of the catalysts, which demonstrated the applicability of the present catalytic system. Such great stability might be thus related to some other features, such as the slower Pd reduction rate and high surface area of the biomass-derived activated carbon, which, together with the incorporation of nitrogen functional

groups, is responsible for the stabilization of Pd nanoparticles and their excellent resistance against leaching under reaction condition (as demonstrated by the almost identical Pd loadings determined in fresh and used catalysts). Furthermore, it should also be mentioned that the catalytic activity displayed by Pd/N-HTC (n.r.) is superior than that shown by a reference catalyst comprised of Pd nanoparticles supported on graphitic carbon nitride (Pd/*g*-C_3N_4), which had a TOF of 761 h^{-1} (on the basis of the total Pd atoms) under identical experimental conditions and it was stable for only one cycle.

It can be also deduced that the experimental protocol used in the synthesis of the catalysts plays an important role in their final stability. In this case, it has been observed that the *in-situ* reduction of the metal nanoparticles performed in Pd/N-HTC (n.r.) gives rise to more stable and active catalysts, which might be attributed to the suppression of additional reducing agent (i.e. $NaBH_4$), which could result in partial poisoning or blocking of the active sites of the surface of the nanoparticles and their long-term stability. The strong interaction between $NaBH_4$ (and its derivatives) and the surface of the nanoparticles is a well-reported aspect.[58] The different reduction rate of the Pd precursor in Pd/N-HTC and Pd/N-HTC (n.r.) might also affect the Pd-N interaction, thus affecting the final catalytic performance of the resulting catalysts.

The excellent stability attained by Pd/N-HTC (n.r.) was further evaluated by performing 6 additional catalytic cycles, so that it was evaluated for a total of 12 consecutive reaction runs. Figure 6 depicts the TOF values (calculated on the basis of surface Pd atoms) achieved by Pd/N-HTC (n.r.) for the 3rd, 6th, 9th and 12th cycle, together with Pd XPS and TEM characterization results registered for the spent catalyst after the 12th reaction cycle.

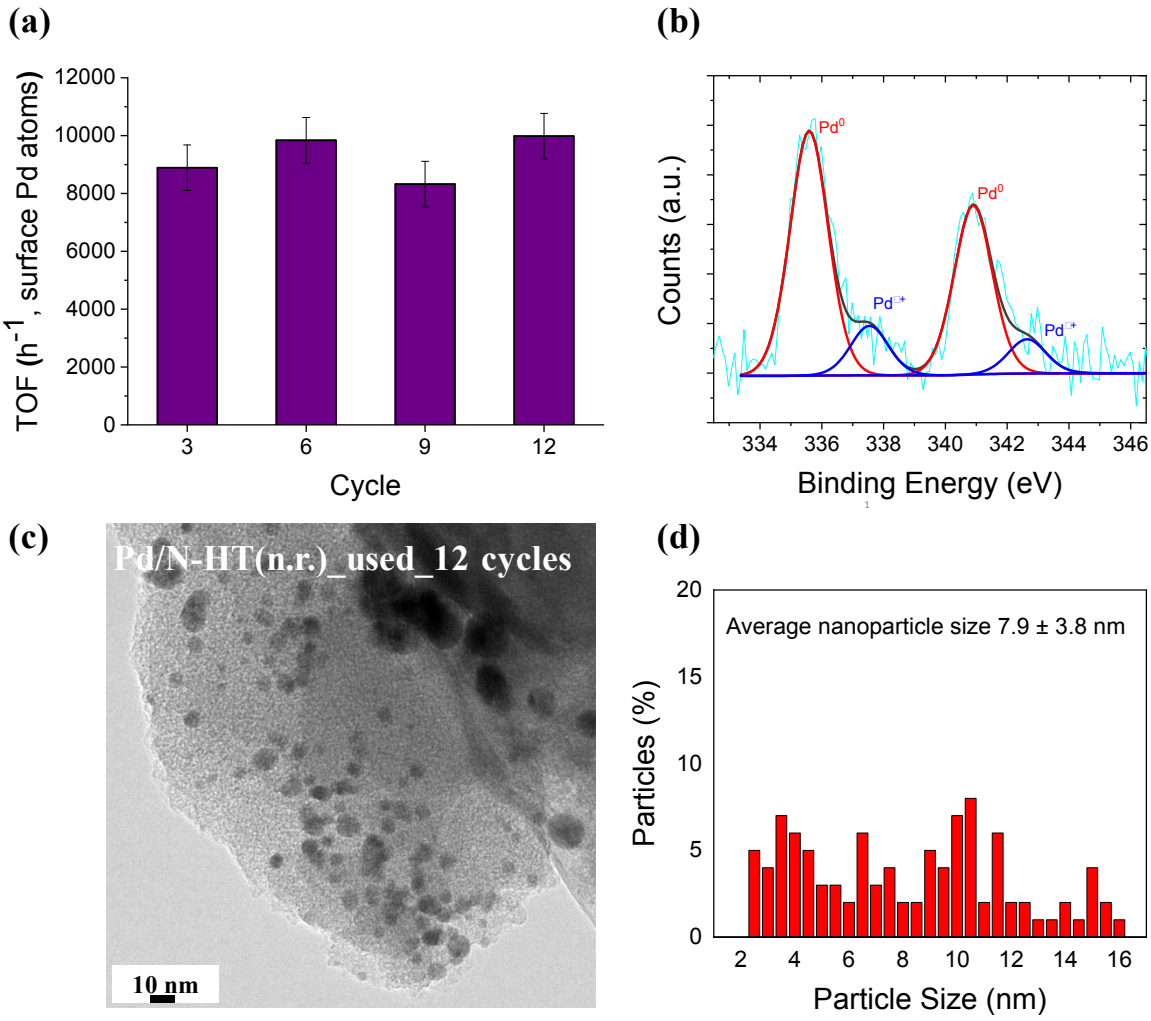

Figure 6. Results achieved for Pd/N-HTC (n.r.) after 12 consecutive reaction cycles: (a) Initial TOF values calculated on the basis of surface Pd atoms; (b) Pd XPS spectrum; (c) TEM micrograph; and (d) histogram with Pd nanoparticle size distributions.

The gas generation profiles registered from the 7th to the 12th cycles indicated that there was a partial loss of the catalytic activity after the 6th run, since the volume of gas generated per mass of catalyst decreased from 734 $mL_{gas}/g_{catalyst}$ in the 6th cycle to 427 $mL_{gas}/g_{catalyst}$ in the 7th cycle and declined further to the 12th cycle in which 332 $mL_{gas}/g_{catalyst}$ were generated. However, it is worth mentioning that the initial catalytic activity of Pd/N-HTC (n.r.) was preserved after the 12 cycles

monitored in this study, as evidenced by the TOF values plotted in Figure 6 (a), which were calculated considering the Pd surface atoms.

The XPS characterization of the spent catalysts (Figure 6 (b)) indicated that there were not changes in the electronic properties of Pd nanoparticles as compared to those determined after the 6th run (i.e. the relative proportion of Pd^0 and Pd^{2+} after 12 cycles was determined to be of 83 and 17 %, respectively, which is nearly identical to those determined after the 6th cycle (82 and 18 %, for Pd^0 and Pd^{2+}, respectively)). ICP analysis after 12 reaction cycles revealed that the final Pd content was of 0.57 wt.%, demonstrating the stability of the nanoparticles against leaching, which may be related to the positive effect of nitrogen functional groups serving as anchorage points.

Concerning the morphology of Pd nanoparticles (Figure 6 (c)), TEM analysis indicated that the nanoparticles preserved their spherical shape, and relatively good dispersion was maintained even after 12 cycles. However, the average nanoparticle size was slightly changed after 12 cycles and it increased up to 7.9 ± 3.8 nm (Figure 6 (d)), compared to the average size determined after the 6th run (6.2 ± 3.8 nm). TOF values and XPS results suggest that there is no poisoning of the catalyst due to any species that may remain chemisorbed and that increase in the average nanoparticle size might be responsible for the partial loss of the catalytic activity expressed as $mL_{gas}/g_{catalyst}$.

The performance of Pd/N-HTC (n.r.) was further evaluated by checking the effect of the reaction temperature and monitoring the reaction at 45, 55, 65, and 75 ºC, and the result of the Arrhenius plot is depicted in Figure 7. The results of the reaction rate were used to determine the apparent activation energy, which was calculated to be of 48.8 kJ/mol.

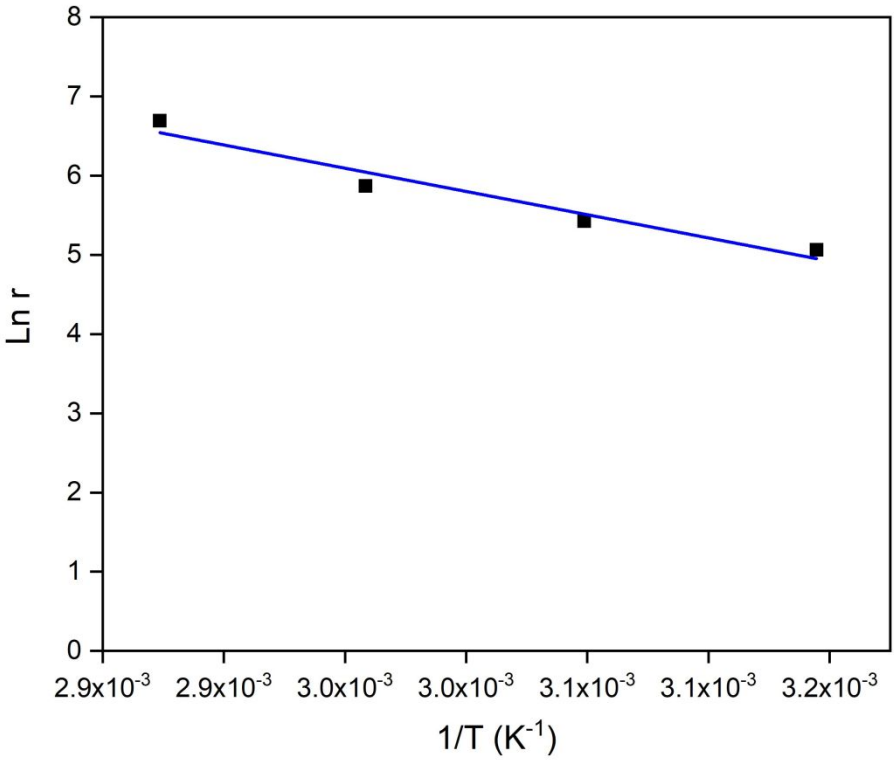

Figure 7. Arrhenius Plot for Pd/N-HTC (n.r.).

One of the most remarkable aspect of the developed catalytic system is its extraordinary stability. To the best of our knowledge, this is an unprecedented work in which the activity of a heterogeneous catalyst is evaluated in the decomposition of formic acid for 12 consecutive catalytic cycles. It should be pointed out that most of the studies barely investigate the stability of the catalysts in more than 5 consecutive cycles. For instance, Yan et al. reported a complex synthesis of a Pd-based catalyst (denoted as AuPd-MnO_x/ZIF-8-rGO), which exhibited an important activity loss, in terms of reaction rate, after 3 consecutive runs.[59] A total activity loss was observed by Navlani-García et al. in the case of PdCo/g-C_3N_4 (1/0.7) after 3 cycles.[60] Zhang et al. reported a bimetallic catalyst based on PdAu nanoparticles (PdAu/C-P) that exhibited high activity; however, the catalyst showed an activity loss of 43 %, expressed as final volume of gas generated, after 3 runs.[61] Du et al. reported a monometallic Pd-based catalyst (Pd/NCt@WO_3),

which showed an important decrease of the reaction rate after 5 cycles.[53] Wang et al. reported that catalysts based on AgPd–MnO_x supported on carbon nanospheres maintained only 82 % of its initial catalytic activity after 5 cycles.[62] Fan et al. observed that the reaction was sluggish after performing 5 consecutive reaction cycles with a catalyst comprising Pd and $Ni(OH)_2$ supported on porous carbon (Pd-$Ni(OH)_2$/PC) and a much longer time was needed to reach the maximum volume of gas evolved in the 6th cycle.[63] Xiang et al. recently reported on a complex catalyst based on Pd and Co_2P nanoparticles supported on N-doped carbon microsheets (Pd-Co_2P/NPC), with a very high Pd loading of 9.81 %, which was claimed to be stable after 7 reaction cycles performed at 50 ºC, but the reaction was progressively sluggish along the monitored cycles.[64]

It should also be mentioned that the experimental conditions used in the tests, such as the reaction time and temperature, also affect the stability of the catalysts (i.e. longer reaction times and higher temperatures are expected to lead to sharper activity decay). For instance, a stable catalyst based on Pd nanoparticles anchored on amino-functionalized hierarchically porous carbon was reported by Wang et al.[65] The stability of that catalyst was evaluated at 25 ºC during 5 cycles which lasted only ~10 min each, which are much milder conditions than those applied in the test monitored in the present study (i.e. 12 consecutive reaction runs of 30 min each, and reaction temperature of 75 ºC). Zhang et al. reported on N-doped activated carbon-supported Pd catalysts,[66] which displayed relatively good stability for 5 consecutive reaction runs at 30 ºC, which are also milder conditions than those used in the present study. Yao et al. evaluated the stability of a catalyst based on Pd nanoparticles assembled on a porous carbon (Co@CN) which derived from ZIF-6 by using mild conditions (i.e. 30 ºC and only 5 cycles).[67] Shokouhimehr et al. evaluated the stability of a catalyst based on nano-sized Pd particles stabilized within the pores of diamine groups grafted open metal site metal-organic frameworks of Cr-MIL-101 (Pd@ED/Cr-MIL-101).[68] It was claimed in that

study that the prepared catalyst was stable, even though its activity was assessed only for 3 cycles. Cai et al. explored the reusability of Pd/C and Pd@Bi/C catalysts by monitoring 3 consecutive runs at 30 ºC and they observed that 50 % of the initial activity (in terms of TOF values) dropped after the 3rd cycle in Pd/C, while Pd@Bi/C attained better stability, but it was only evaluated during 3 runs.[69]

Another aspect which deserves mention is the high TOF values achieved by Pd/N-HTC (n.r.) (average TOF of 8365 h^{-1} calculated for the 2nd reaction cycle and on the basis of the surface Pd atoms, which maintains for 12 cycles), which is among the highest value ever reported for Pd-based catalysts.[21,70] It should also be considered that the higher TOF values achieved by most of the catalysts reported elsewhere are linked to the use of bimetallic or multimetallic nanoparticles, which usually contain other noble metal, such as Ag and/or Au.[71] Upon Pd alloying, some of the effects responsible for the deactivation of the catalysts (i.e. adsorption of poisonous intermediates) are partially alleviated by modulation of the surface properties and composition.[21,72] However, the preparation of bimetallic and multimetallic catalysts usually requires more complex experimental protocols, such as consecutive reductions of the metal precursor, galvanic replacement, etc.,[73,74] thus achieving stable monometallic catalysts for the present application is highly desirable yet challenging. This reinforces the remarkable performance of the catalysts developed in this study.

The assessment and comparison of the activity and stability of the catalysts is not straightforward, since neither benchmark experimental conditions nor benchmark catalysts for the decomposition of formic acid are stablished so far in the literature. In order to make a proper assessment of the achievements of our Pd/N-HTC (n.r.) catalyst, Table 3 compiles a summary of many representative catalysts evaluated in the decomposition of formic acid. Details of the properties of the catalysts (metal loading and nanoparticle size), the experimental conditions

(reaction temperature, $n_{metal}/n_{FA,}$ and presence of additives) and the criteria followed in the calculation of the TOF values (surface metal atoms or total metal atoms) are indicated in Table 3.

Table 3. Comparison of the catalytic performance of some representative Pd-based catalysts.

Catalyst	Metal (loading) [wt%]	NP Size [nm]	T [ºC]	n_{metal}/n_{FA}	Additive	TOF $[h^{-1}]$[a)]	Ea [kJ mol^{-1}]	Ref.
Pd/N-HTC (n.r.)	Pd (0.72)	3.1 ± 1.4	75	0.001	HCOONa	1214[b)] 8365[c)]	48.8	This study
Pd/MSC-30	Pd (9.6)	2.3 ± 0.4	50	0.01	HCOONa	2623[d, e)]	39.1	[75]
Pd/N-MSC-30	Pd (4.0)	1.4	60	0.02	HCOONa	8414[d)]	43.7	[76]
$Pd/CN_{0.25}$	Pd (10)	3.1	25	0.0075	None	5530[f)] 752[e)]	48.8	[77]
Pd@CN	Pd (8.0)	4.0	15	0.0015	None	71	-	[78]
Pd/C_m	Pd (6.0)	1.4 ± 0.3	60	0.006	HCOONa	7256[e)]	39.6	[79]
$Pd/NC_{400}@WO_3$	Pd (0.44)	2.3 ± 0.2	50	0.004	HCOONa	1225	37.03	[53]
Pd/APC	Pd (4.58)	2.3	50	0.011	HCOONa	2230	46.31	[80]
Pd/HTNC-950	Pd (4.68)	2.8 ± 0.7	30	0.0021	HCOONa	1631[e)]	33.67	[66]
Pd/NMC-400	Pd (3.2)	2.7 ± 0.6	25	0.0009	None	913	36.86	[81]
$Pd/C_{ZIF\text{-}8\text{-}950}$	Pd (3.325)	3.02 ± 0.02	30	0.0028	HCOONa	1166[d)]	34.9	[82]
$Pd/NHPC\text{-}NH_2$	Pd (5.8)	2.5	25	0.01	None	1265[e)] 3798[f)]	46.3	[65]
Pd/NHPC-AC	Pd (2.7)	1.88 ± 0.48	60	0.0057	HCOONa	4115	21.5	[83]
Pd@CN900K	Pd (9.3)	1.1 ± 0.2	60	0.017	HCOONa	14400[d, e)]	46.9	[84]
Pd/C	Pd (2.3)	2.1 ± 0.3	25	0.004	HCOONa	835[f)]	48.0	[85]
Pd-CNTs-in	Pd (4.69)	4.2 ± 0.8	30	0.0042	HCOONa	1135[f)]	36.60	[86]
$Pd/mpg\text{-}C_3N_4$	Pd (9.5)	1.7 ± 0.49	25	0.0045	None	144	29.1	[87]
Pd@TU-PMO	Pd (3.7)	2.3	80	0.0021	None	32	63	[88]
SBA-15-Amine/Pd	Pd (3.4)	1.9	26	0.0016	None	293	-	[89]
$Pd/NH_2\text{-}MIL\text{-}125$	Pd (0.5)	3.1	32	0.00023	HCOONa	214[e)]	-	[90]
Pd/POP-2	Pd (3.1)	3.7 ± 0.5	60	0.03	None	167	66.76	[91]

Au_2Pd_8/SBA-15-Amine	Au (3.69) Pd (9.04)	4.5 ± 0.5	50	0.035	HCOONa	1786[e)]	47.6	[92]
Ag_1Pd_9/NPC	Ag (0.97) Pd (9.03)	3.5	50	0.02	HCOONa	3000	44.48	[93]
$Co_{48}Au_5Pd_{47}$@MIL-101-NH_2	Co (2.33) Au (0.71) Pd (4.14)	2.5	50	0.027	HCOONa	361[f)]	67.1	[94]
Au_3Pd_1/C	Au (48.23) Pd (8.70)	4.18	92	-	NH_4HCO_2	407.5[e)]	23.3	[95]
$Ag_{10}Pd_{90}$/0.2CND/SBA-15	Ag (0.93) Pd (9.26)	4.5 ± 0.5	50	0.032	HCOONa	893	43.2	[96]
0.8Pd0.2Ni$(OH)_2$@S-1	Pd (0.56) Ni (0.08)	1.7	60	0.012	None	5803	52.4	[97]

a) TOF values calculated on the initial time or initial conversion of formic acid; b) TOF value calculated for the 2nd reaction run and considering the total Pd atoms; c) TOF value calculated for the 2nd reaction run and considering surface Pd atoms; d)TOF values calculated on the complete time of gas generation; e)TOF values calculated on basis of the noble metal atoms; f)TOF values calculated on the basis of surface metal sites.

The superiority of the developed Pd/N-HTC (n.r.) is not only evidenced by its excellent catalytic activity and stability over 6 consecutive reaction cycles, but also from the easy experimental protocol used in its synthesis and the sustainable approach followed. In this line, the synthesis method proposed in this study to prepare the catalytic support involves an environmentally friendly process using biomass residues as a precursor, which afforded an activated carbon with excellent properties. It is important to highlight the interest of using biomass residues as raw materials to obtain high added value products, since this is a very interesting alternative to reduce production costs and environmental problems. The use of biomass residues as a precursor to obtain activated carbons has widely been explored. However, harsher experimental conditions, as well as activating agents with high concentrations and protocols with more steps, are traditionally employed.[83,98–102] The protocol herein used comprises a HTC process, which contributes to the effective concentration of organic matter and carbon precursors are converted into valuable materials using processes at low temperatures and under self-generated pressures, and possesses notable advantages from the practical view point while being an environmentally friendly process.[32,103,104] In the present study, a HTC synthesis was combined with a chemical activation process, producing

higher yields and better development of porosity. Low-concentrated H_3PO_4 was used in this case because it has positive aspects compared to other chemical activation agents, such as lower polluting effect, which is further reduced when low concentrations are used, which in turns reduced also the final cost of the material.[32,105–107] As for the functionalization with nitrogen groups, an organic reaction was used in mild conditions at low temperature and avoiding the previous oxidation process, which allowed the introduction of nitrogen functional groups preserving the porous texture characteristic of the pristine activated carbon. Generally, chemical functionalization to introduce nitrogen functional groups requires more complex experimental protocols with high temperatures, more aggressive conditions, and more experimental steps.[57,84,93,108–110] Common synthesis methods involve CVD (chemical vapor deposition), carbonization of N containing sources and electrochemical functionalization.[111,112] All these aspects make the proposed synthesis of activated carbon a promising alternative from the industrial point of view to produce biomass carbon materials of high yield and low cost, providing an important contribution in the sector of renewable energy.

In addition, the superiority of the system herein studied is not only evidenced by its impressive stability under reaction conditions, but also by the straightforward method used for the synthesis of the catalyst, in which the pre-reduction step with an additional agent such as $NaBH_4$ is not required. Moreover, it should be also pointed out that no additional thermal or washing treatment was performed between two consecutive cycles, and the spent catalyst was easily collected from the reactor by filtration, thus emphasizing its practicality over all the homogeneous catalysts and, more important, over most of the heterogeneous catalytic systems previously studied, in which a lack of stability is reported or additional treatments of the catalysts are necessary for their regeneration.[113]Moreover, it should be also highlighted that the resulting Pd/N-HTC (n.r.) catalyst

is competitive cost-wise, not only because a biomass precursor is used for the synthesis of the support and the resulting catalyst can be reused during several times without showing significant activity decay, but also because it has a much lower Pd loading compared to most of the catalysts reported in other studies (See Table 3).

Conclusions

Pd-based N-doped activated carbon catalysts were prepared by a H_3PO_4-assisted hydrothermal carbonization of a hemp residue followed by nitrogen functionalization and impregnation with the Pd precursor and their activity in the production of hydrogen from formic acid was assessed. Catalysts with promising activity and excellent stability were achieved, which was related to both the properties of the catalysts and the synthetic protocol used. Among investigated, Pd/N-HTC (n.r.) catalyst, in which no pre-reduction step was carried out, displayed excellent stability even after 6 consecutive reaction cycles. Further insight on the stability of Pd/N-HTC (n.r.) were achieved by performing 6 additional catalytic cycles, so that its stability was assessed in a total of 12 consecutive reaction cycles, which is an unprecedented evaluation of the stability of the catalysts used in the dehydrogenation of formic acid. The results of those tests revealed that the initial activity of Pd/N-HTC (n.r.) was preserved along the 12 consecutive cycles. That characteristic, together with the high TOF value achieved by Pd/N-HTC (n.r.) (TOF of 8365 h^{-1} calculated for the 2^{nd} reaction cycle and on the basis of the surface Pd atoms) makes the present catalytic system a very interesting candidate for the efficient hydrogen production from formic and with great commercial application potential.

The results herein obtained are expected to motivate further efforts towards the design and development of new biomass-derived metal-based catalysts as an auspicious option of biomass

upgrading, which is a crucial aspect in the desirable sustainable energy and environmental scenarios.

AUTHOR INFORMATION

***Corresponding Author:** Diego Cazorla-Amorós, Departamento de Química Inorgánica e Instituto Universitario de Materiales, University of Alicante, P.O. Box 99, San Vicente del Raspeig, E-03080, Alicante, Spain. Phone number: +34965903946; Email: cazorla@ua.es

Author Contributions

The manuscript was written through contributions of all authors. All authors have given approval to the final version of the manuscript.

Notes

The authors declare no competing financial interest.

ACKNOWLEDGMENT

This work was financed by the MICINN, FEDER (RTI2018-095291-B-I00). JCG thanks for her predoctoral scholarship (GRISOLIA / 2018/105) funded by the Generalitat Valenciana. MNG thanks the Plan GenT project (CDEIGENT / 2018/027) for the financial support. DST thanks MICINN for the "Juan de la Cierva" contract (IJCI-2016-27636).

REFERENCES

(1) Höök, M.; Tang, X. Depletion of Fossil Fuels and Anthropogenic Climate Change—A Review. *Energy Policy* **2013**, *52*, 797–809. https://doi.org/10.1016/J.ENPOL.2012.10.046.

(2) IPCC, 2014: Climate Change 2014: Synthesis Report. Contribution of Working Groups I, II and III to the Fifth Assessment Report of the Intergovernmental Panel on Climate Change [Core Writing Team, R.K. Pachauri and L.A. Meyer (eds.)]. IPCC, Geneva, Switzer. https://doi.org/https://www.ipcc.ch/report/ar5/syr/.

(3) Masson-Delmotte, V.; Zhai, P.; Pörtner, H.-O.; Roberts, D.; Skea, J.; Shukla, P. R.; Pirami, A.; Moufouma-Okia, W.; Péan, C.; Pidcock, R.; et al. Global Warming of 1.5°C. An IPCC Special Report on the impacts of global warming of 1.5°C above pre-industrial levels and related global greenhouse gas emission pathways, in the context of strengthening the global response to the threat of climate change. https://doi.org/https://www.ipcc.ch/sr15/download/#full.

(4) Mika, L. T.; Cséfalvay, E.; Németh, Á. Catalytic Conversion of Carbohydrates to Initial Platform Chemicals: Chemistry and Sustainability. *Chem. Rev.* **2018**, *118* (2), 505–613. https://doi.org/10.1021/acs.chemrev.7b00395.

(5) Pileidis, F. D.; Titirici, M.-M. Levulinic Acid Biorefineries: New Challenges for Efficient Utilization of Biomass. *ChemSusChem* **2016**, *9* (6), 562–582. https://doi.org/10.1002/cssc.201501405.

(6) Luterbacher, J. S.; Martin Alonso, D.; Dumesic, J. A. Targeted Chemical Upgrading of Lignocellulosic Biomass to Platform Molecules. *Green Chem.* **2014**, *16* (12), 4816–4838. https://doi.org/10.1039/C4GC01160K.

(7) Dahiya, S.; Kumar, A. N.; Shanthi Sravan, J.; Chatterjee, S.; Sarkar, O.; Mohan, S. V. Food Waste Biorefinery: Sustainable Strategy for Circular Bioeconomy. *Bioresour. Technol.*

2018, *248*, 2–12. https://doi.org/10.1016/j.biortech.2017.07.176.

(8) Schutyser, W.; Renders, T.; den Bosch, S.; Koelewijn, S.-F.; Beckham, G. T.; Sels, B. F. Chemicals from Lignin: An Interplay of Lignocellulose Fractionation, Depolymerisation, and Upgrading. *Chem. Soc. Rev.* **2018**, *47* (3), 852–908. https://doi.org/10.1039/C7CS00566K.

(9) Bulushev, D. A.; Ross, J. R. H. Towards Sustainable Production of Formic Acid. *ChemSusChem* **2018**, *11* (5), 821–836. https://doi.org/doi:10.1002/cssc.201702075.

(10) Chen, X.; Liu, Y.; Wu, J. Sustainable Production of Formic Acid from Biomass and Carbon Dioxide. *Mol. Catal.* **2020**, *483*, 110716. https://doi.org/10.1016/J.MCAT.2019.110716.

(11) Yu, X.; Pickup, P. G. Recent Advances in Direct Formic Acid Fuel Cells (DFAFC). *J. Power Sources* **2008**, *182* (1), 124–132. https://doi.org/10.1016/J.JPOWSOUR.2008.03.075.

(12) van Putten, R.; Wissink, T.; Swinkels, T.; Pidko, E. A. Fuelling the Hydrogen Economy: Scale-up of an Integrated Formic Acid-to-Power System. *Int. J. Hydrogen Energy* **2019**, *44* (53), 28533–28541. https://doi.org/10.1016/J.IJHYDENE.2019.01.153.

(13) Deng, L.; Zhao, Y.; Li, J.; Fu, Y.; Liao, B.; Guo, Q.-X. Conversion of Levulinic Acid and Formic Acid into γ-Valerolactone over Heterogeneous Catalysts. *ChemSusChem* **2010**, *3* (10), 1172–1175. https://doi.org/doi:10.1002/cssc.201000163.

(14) De, S.; Gevers, L.; Emwas, A.-H.; Gascon, J. Conversion of Formic Acid into Methanol Using a Bipyridine-Functionalized Molecular Heterogeneous Catalyst. *ACS Sustain. Chem.*

Eng. **2019**, *7* (4), 3933–3939. https://doi.org/10.1021/acssuschemeng.8b05070.

(15) Navlani-García, M.; Mori, K.; Nozaki, A.; Kuwahara, Y.; Yamashita, H. Investigation of Size Sensitivity in the Hydrogen Production from Formic Acid over Carbon-Supported Pd Nanoparticles. *ChemistrySelect* **2016**, *1* (9), 1879–1886. https://doi.org/10.1002/slct.201600559.

(16) Navlani-García, M.; Mori, K.; Salinas-Torres, D.; Kuwahara, Y.; Yamashita, H. New Approaches Toward the Hydrogen Production From Formic Acid Dehydrogenation Over Pd-Based Heterogeneous Catalysts. *Front. Mater.* **2019**, *6*, 44. https://doi.org/10.3389/fmats.2019.00044.

(17) Navlani-García, M.; Mori, K.; Nozaki, A.; Kuwahara, Y.; Yamashita, H. Screening of Carbon-Supported PdAg Nanoparticles in the Hydrogen Production from Formic Acid. *Ind. Eng. Chem. Res.* **2016**, *55* (28), 7612–7620. https://doi.org/10.1021/acs.iecr.6b01635.

(18) Wen, M.; Mori, K.; Futamura, Y.; Kuwahara, Y.; Navlani-García, M.; An, T.; Yamashita, H. PdAg Nanoparticles within Core-Shell Structured Zeolitic Imidazolate Framework as a Dual Catalyst for Formic Acid-Based Hydrogen Storage/Production. *Sci. Rep.* **2019**, *9* (1), 15675. https://doi.org/10.1038/s41598-019-52133-5.

(19) Navlani-García, M.; Salinas-Torres, D.; Cazorla-Amorós, D. Hydrogen Production from Formic Acid Attained by Bimetallic Heterogeneous Pdag Catalytic Systems. *Energies* **2019**, *12* (21), 1–27. https://doi.org/10.3390/en12214027.

(20) Navlani-García, M.; Salinas-Torres, D.; Mori, K.; Kuwahara, Y.; Yamashita, H. Photocatalytic Approaches for Hydrogen Production via Formic Acid Decomposition. *Top.*

Curr. Chem. **2019**, *377* (5), 27. https://doi.org/10.1007/s41061-019-0253-4.

(21) Navlani-García, M.; Mori, K.; Kuwahara, Y.; Yamashita, H. Recent Strategies Targeting Efficient Hydrogen Production from Chemical Hydrogen Storage Materials over Carbon-Supported Catalysts. *NPG Asia Mater.* **2018**, 1–16. https://doi.org/10.1038/s41427-018-0025-6.

(22) DOE Techical Targets for Onboard Hydrogen Storage for Light-Duty Vehicles. https://www.energy.gov/eere/fuelcells/doe-technical-targets-onboard-hydrogen-storage-light-duty-vehicles (accessed 06th August 2020).

(23) Bulushev, D. A.; Bulusheva, L. G.; Beloshapkin, S.; O'Connor, T.; Okotrub, A. V.; Ryan, K. M. Pd Clusters Supported on Amorphous, Low-Porosity Carbon Spheres for Hydrogen Production from Formic Acid. *ACS Appl. Mater. Interfaces* **2015**, *7* (16), 8719–8726. https://doi.org/10.1021/acsami.5b00983.

(24) García-Aguilar, J.; Navlani-García, M.; Berenguer-Murcia, Á.; Mori, K.; Kuwahara, Y.; Yamashita, H.; Cazorla-Amorós, D. Evolution of the PVP-Pd Surface Interaction in Nanoparticles through the Case Study of Formic Acid Decomposition. *Langmuir* **2016**, *32* (46), 12110–12118. https://doi.org/10.1021/acs.langmuir.6b03149.

(25) Wu, Y.; Wen, M.; Navlani-García, M.; Kuwahara, Y.; Mori, K.; Yamashita, H. Palladium Nanoparticles Supported on Titanium Doped Graphitic Carbon Nitride for Formic Acid Dehydrogenation. *Chem. - An Asian J.* **2017**, *12*, 860–867. https://doi.org/10.1002/asia.201700041.

(26) Navlani-García, M.; Salinas-Torres, D.; Mori, K.; Léonard, A. F.; Kuwahara, Y.; Job, N.;

Yamashita, H. Insights on Palladium Decorated Nitrogen-Doped Carbon Xerogels for the Hydrogen Production from Formic Acid. *Catal. Today* **2019**, *324*, 90–96. https://doi.org/10.1016/j.cattod.2018.06.013.

(27) Zhang, C.; Leng, Y.; Jiang, P.; Li, J.; Du, S. Immobilizing Palladium Nanoparticles on Nitrogen-Doped Carbon for Promotion of Formic Acid Dehydrogenation and Alkene Hydrogenation. *ChemistrySelect* **2017**, *2* (20), 5469–5474. https://doi.org/10.1002/slct.201701176.

(28) Bi, Q. Y.; Lin, J. D.; Liu, Y. M.; He, H. Y.; Huang, F. Q.; Cao, Y. Dehydrogenation of Formic Acid at Room Temperature: Boosting Palladium Nanoparticle Efficiency by Coupling with Pyridinic-Nitrogen-Doped Carbon. *Angew. Chemie - Int. Ed.* **2016**, *55* (39), 11849–11853. https://doi.org/10.1002/anie.201605961.

(29) Bulushev, D. A.; Zacharska, M.; Shlyakhova, E. V; Chuvilin, A. L.; Guo, Y.; Beloshapkin, S.; Okotrub, A. V; Bulusheva, L. G. Single Isolated Pd^{2+} Cations Supported on N-Doped Carbon as Active Sites for Hydrogen Production from Formic Acid Decomposition. *ACS Catal.* **2016**, *6* (2), 681–691. https://doi.org/10.1021/acscatal.5b02381.

(30) Falco, C.; Sieben, J. M.; Brun, N.; Sevilla, M.; Van Der Mauelen, T.; Morallón, E.; Cazorla-Amorós, D.; Titirici, M.-M. Hydrothermal Carbons from Hemicellulose-Derived Aqueous Hydrolysis Products as Electrode Materials for Supercapacitors. *ChemSusChem* **2013**, *6* (2), 374–382. https://doi.org/10.1002/cssc.201200817.

(31) Falco, C.; Marco-Lozar, J. P.; Salinas-Torres, D.; Morallón, E.; Cazorla-Amorós, D.; Titirici, M. M.; Lozano-Castelló, D. Tailoring the Porosity of Chemically Activated

Hydrothermal Carbons: Influence of the Precursor and Hydrothermal Carbonization Temperature. *Carbon.* **2013**, *62*, 346–355. https://doi.org/10.1016/j.carbon.2013.06.017.

(32) Quesada-Plata, F.; Ruiz-Rosas, R.; Morallón, E.; Cazorla-Amorós, D. Activated Carbons Prepared through H_3PO_4-Assisted Hydrothermal Carbonisation from Biomass Wastes: Porous Texture and Electrochemical Performance. *Chempluschem* **2016**, *81* (12), 1349–1359. https://doi.org/10.1002/cplu.201600412.

(33) Bi, Z.; Kong, Q.; Cao, Y.; Sun, G.; Su, F.; Wei, X.; Li, X.; Ahmad, A.; Xie, L.; Chen, C.-M. Biomass-Derived Porous Carbon Materials with Different Dimensions for Supercapacitor Electrodes: A Review. *J. Mater. Chem. A* **2019**, *7* (27), 16028–16045. https://doi.org/10.1039/C9TA04436A.

(34) Titirici, M. M.; White, R. J.; Brun, N.; Budarin, V. L.; Su, D. S.; Del Monte, F.; Clark, J. H.; MacLachlan, M. J. Sustainable Carbon Materials. *Chem. Soc. Rev.* **2015**, *44* (1), 250–290. https://doi.org/10.1039/c4cs00232f.

(35) Ruiz-Rosas, R.; Valero-Romero, M. J.; Salinas-Torres, D.; Rodríguez-Mirasol, J.; Cordero, T.; Morallón, E.; Cazorla-Amorós, D. Electrochemical Performance of Hierarchical Porous Carbon Materials Obtained from the Infiltration of Lignin into Zeolite Templates. *ChemSusChem* **2014**, *7* (5), 1458–1467. https://doi.org/10.1002/cssc.201301408.

(36) Deng, J.; Li, M.; Wang, Y. Biomass-Derived Carbon: Synthesis and Applications in Energy Storage and Conversion. *Green Chem.* **2016**, *18* (18), 4824–4854. https://doi.org/10.1039/C6GC01172A.

(37) De, S.; Balu, A. M.; Van Der Waal, J. C.; Luque, R. Biomass-Derived Porous Carbon

Materials: Synthesis and Catalytic Applications. *ChemCatChem* **2015**, *7* (11), 1608–1629. https://doi.org/10.1002/cctc.201500081.

(38) Sevilla, M.; Gu, W.; Falco, C.; Titirici, M. M.; Fuertes, A. B.; Yushin, G. Hydrothermal Synthesis of Microalgae-Derived Microporous Carbons for Electrochemical Capacitors. *J. Power Sources* **2014**, *267*, 26–32. https://doi.org/10.1016/j.jpowsour.2014.05.046.

(39) Mostazo-López, M. J.; Ruiz-Rosas, R.; Morallón, E.; Cazorla-Amorós, D. Nitrogen Doped Superporous Carbon Prepared by a Mild Method. Enhancement of Supercapacitor Performance. *Int. J. Hydrogen Energy* **2016**, *41* (43), 19691–19701. https://doi.org/10.1016/j.ijhydene.2016.03.091.

(40) Thommes, M.; Kaneko, K.; Neimark, A. V.; Olivier, J. P.; Rodriguez-Reinoso, F.; Rouquerol, J.; Sing, K. S. W. Physisorption of Gases, with Special Reference to the Evaluation of Surface Area and Pore Size Distribution (IUPAC Technical Report). *Pure Appl. Chem.* **2015**. https://doi.org/10.1515/pac-2014-1117.

(41) Jagiello, J.; Olivier, J. P. 2D-NLDFT Adsorption Models for Carbon Slit-Shaped Pores with Surface Energetical Heterogeneity and Geometrical Corrugation. *Carbon.* **2013**, *55*, 70–80. https://doi.org/10.1016/j.carbon.2012.12.011.

(42) Domínguez-Domínguez, S.; Berenguer-Murcia, A.; Pradhan, B. K.; Linares-Solano, A.; Cazorla-Amorós, D. Semihydrogenation of Phenylacetylene Catalyzed by Palladium Nanoparticles Supported on Carbon Materials. *J. Phys. Chem. C* **2008**, *112* (10), 3827–3834. https://doi.org/10.1021/jp710693u.

(43) Wu, J.; Wang, K.; Li, Y.; Yu, P. Semihydrogenation of Phenylacetylene Catalyzed by

Palladium Nanoparticles Supported on Organic Group Modified Silica. In *Advanced Materials Research*; 2011; Vol. 233–235, pp 2109–2112. https://doi.org/10.4028/www.scientific.net/AMR.233-235.2109.

(44) Navlani-García, M.; Mori, K.; Wen, M.; Kuwahara, Y.; Yamshita, H. Size Effect of Carbon-Supported Pd Nanoparticles in the Hydrogen Production from Formic Acid. *Bull. Chem. Soc. Jpn.* **2015**, *1370* (10), 78–80. https://doi.org/10.1080/03758397.1955.10857269.

(45) Zhang, S.; Jiang, B.; Jiang, K.; Cai, W. Bin. Surfactant-Free Synthesis of Carbon-Supported Palladium Nanoparticles and Size-Dependent Hydrogen Production from Formic Acid-Formate Solution. *ACS Appl. Mater. Interfaces* **2017**, *9* (29), 24678–24687. https://doi.org/10.1021/acsami.7b08441.

(46) Salinas-Torres, D.; Léonard, A. F.; Stergiopoulos, V.; Busby, Y.; Pireaux, J. J.; Job, N. Effect of Nitrogen Doping on the Pore Texture of Carbon Xerogels Based on Resorcinol-Melamine-Formaldehyde Precursors. *Microporous Mesoporous Mater.* **2018**, *256*, 190–198. https://doi.org/10.1016/j.micromeso.2017.08.004.

(47) Deraedt, C.; Salmon, L.; Gatard, S.; Ciganda, R.; Hernandez, R.; Ruiz, J.; Astruc, D. Sodium Borohydride Stabilizes Very Active Gold Nanoparticle Catalysts. *Chem. Commun.* **2014**, *50* (91), 14194–14196. https://doi.org/10.1039/C4CC05946H.

(48) Polte, J. Fundamental Growth Principles of Colloidal Metal Nanoparticles – a New Perspective. *CrystEngComm* **2015**, *17* (36), 6809–6830. https://doi.org/10.1039/C5CE01014D.

(49) Yin, Y.; Alivisatos, A. P. Colloidal Nanocrystal Synthesis and the Organic-Inorganic

Interface. *Nature* **2005**, *437* (7059), 664–670. https://doi.org/10.1038/nature04165.

(50) Jeon, M.; Han, D. J.; Lee, K. S.; Choi, S. H.; Han, J.; Nam, S. W.; Jang, S. C.; Park, H. S.; Yoon, C. W. Electronically Modified Pd Catalysts Supported on N-Doped Carbon for the Dehydrogenation of Formic Acid. *Int. J. Hydrogen Energy* **2016**, *41* (34), 15453–15461. https://doi.org/10.1016/j.ijhydene.2016.04.102.

(51) Ortega-Murcia, A.; Navlani-García, M.; Morallón, E.; Cazorla-Amorós, D. MWCNT-Supported PVP-Capped Pd Nanoparticles as Efficient Catalysts for the Dehydrogenation of Formic Acid. *Front. Chem.* **2020**, *8*, 359. https://doi.org/10.3389/fchem.2020.00359.

(52) Golub, F. S.; Beloshapkin, S.; Gusel'nikov, A. V.; Bolotov, V. A.; Parmon, V. N.; Bulushev, D. A. Boosting Hydrogen Production from Formic Acid over Pd Catalysts by Deposition of N-Containing Precursors on the Carbon Support. *Energies* **2019**, *12* (20), 3885. https://doi.org/10.3390/en12203885.

(53) Du, S.; Zhang, C.; Jiang, P.; Leng, Y. Palladium Nanoparticles Immobilized on Nitride Carbon-Coated Mesoporous Tungsten Oxide for Formic Acid Dehydrogenation. *ACS Appl. Nano Mater.* **2019**, *2* (11), 7432–7440. https://doi.org/10.1021/acsanm.9b01956.

(54) Wang, C.-A.; Nie, K.; Song, G.-D.; Li, Y.-W.; Han, Y.-F. Phenanthroline-Based Microporous Organic Polymer as a Platform for an Immobilized Palladium Catalyst for Organic Transformations. *RSC Adv.* **2019**, *9* (15), 8239–8245. https://doi.org/10.1039/C9RA00460B.

(55) Mori, K.; Dojo, M.; Yamashita, H. Pd and Pd-Ag Nanoparticles within a Macroreticular Basic Resin: An Efficient Catalyst for Hydrogen Production from Formic Acid

Decomposition. *ACS Catal.* **2013**, *3* (6), 1114–1119. https://doi.org/10.1021/cs400148n.

(56) Lv, Q.; Meng, Q.; Liu, W.; Sun, N.; Jiang, K.; Ma, L.; Peng, Z.; Cai, W.; Liu, C.; Ge, J.; et al. Pd–PdO Interface as Active Site for HCOOH Selective Dehydrogenation at Ambient Condition. *J. Phys. Chem. C* **2018**, *122* (4), 2081–2088. https://doi.org/10.1021/acs.jpcc.7b08105.

(57) Mostazo-López, M. J.; Ruiz-Rosas, R.; Morallón, E.; Cazorla-Amorós, D. Generation of Nitrogen Functionalities on Activated Carbons by Amidation Reactions and Hofmann Rearrangement: Chemical and Electrochemical Characterization. *Carbon.* **2015**, *91*, 252–265. https://doi.org/10.1016/j.carbon.2015.04.089.

(58) Ansar, S. M.; Ameer, F. S.; Hu, W.; Zou, S.; Pittman, C. U.; Zhang, D. Removal of Molecular Adsorbates on Gold Nanoparticles Using Sodium Borohydride in Water. *Nano Lett.* **2013**, *13* (3), 1226–1229. https://doi.org/10.1021/nl304703w.

(59) Yan, J.-M.; Wang, Z.-L.; Gu, L.; Li, S.-J.; Wang, H.-L.; Zheng, W.-T.; Jiang, Q. AuPd–MnOx/MOF–Graphene: An Efficient Catalyst for Hydrogen Production from Formic Acid at Room Temperature. *Adv. Energy Mater.* **2015**, *5* (10), 1500107. https://doi.org/10.1002/aenm.201500107.

(60) Navlani-García, M.; Salinas-Torres, D.; Mori, K.; Kuwahara, Y.; Yamashita, H. Enhanced Formic Acid Dehydrogenation by the Synergistic Alloying Effect of PdCo Catalysts Supported on Graphitic Carbon Nitride. *Int. J. Hydrogen Energy* **2018**. https://doi.org/10.1016/j.ijhydene.2018.11.057.

(61) Zhang, J.; Wang, H.; Zhao, Q.; Di, L.; Zhang, X. Facile Synthesis of PdAu/C by Cold

Plasma for Efficient Dehydrogenation of Formic Acid. *Int. J. Hydrogen Energy* **2020**, *45* (16), 9624–9634. https://doi.org/10.1016/j.ijhydene.2020.01.196.

(62) Zhang, X.; Shang, N.; Zhou, X.; Feng, C.; Gao, S.; Wu, Q.; Wang, Z.; Wang, C. AgPd-MnOxsupported on Carbon Nanospheres: An Efficient Catalyst for Dehydrogenation of Formic Acid. *New J. Chem.* **2017**, *41* (9), 3443–3449. https://doi.org/10.1039/c6nj03873e.

(63) Dong, Y.; Chen, Q.; Qiu, C.; Ma, X.; Wang, Y.; Sun, T.; Fan, G. Synergistic Catalysis of Pd–Ni(OH)2 Hybrid Anchored on Porous Carbon for Hydrogen Evolution from the Dehydrogenation of Formic Acid. *Int. J. Hydrogen Energy* **2020**, *45* (23), 12849–12858. https://doi.org/https://doi.org/10.1016/j.ijhydene.2020.03.016.

(64) Duan, J.; Xiang, Z.; Zhang, H.; Zhang, B.; Xiang, X. Pd-Co2P Nanoparticles Supported on N-Doped Biomass-Based Carbon Microsheet with Excellent Catalytic Performance for Hydrogen Evolution from Formic Acid. *Appl. Surf. Sci.* **2020**, *530*, 147191. https://doi.org/https://doi.org/10.1016/j.apsusc.2020.147191.

(65) Wang, Z.; Wang, C.; Mao, S.; Gong, Y.; Chen, Y.; Wang, Y. Pd Nanoparticles Anchored on Amino-Functionalized Hierarchically Porous Carbon for Efficient Dehydrogenation of Formic Acid under Ambient Conditions. *J. Mater. Chem. A* **2019**, *7* (45), 25791–25795. https://doi.org/10.1039/C9TA10196A.

(66) Yao, M.; Liang, W.; Chen, H.; Zhang, X. Efficient Hydrogen Production from Formic Acid Using Nitrogen-Doped Activated Carbon Supported Pd. *Catal. Letters* **2020**, *150* (8), 2377–2384. https://doi.org/10.1007/s10562-020-03141-y.

(67) Yao, M.; Ye, Y.; Chen, H.; Zhang, X. Pd Supported on Co@CN Derived from ZIF-67 as

Catalyst for Hydrogen Generation from Formic Acid. *Mater. Lett.* **2020**, *264*, 127308. https://doi.org/https://doi.org/10.1016/j.matlet.2020.127308.

(68) Alamgholiloo, H.; Rostamnia, S.; Hassankhani, A.; Liu, X.; Eftekhari, A.; Hasanzadeh, A.; Zhang, K.; Karimi-Maleh, H.; Khaksar, S.; Varma, R. S.; et al. Formation and Stabilization of Colloidal Ultra-Small Palladium Nanoparticles on Diamine-Modified Cr-MIL-101: Synergic Boost to Hydrogen Production from Formic Acid. *J. Colloid Interface Sci.* **2020**, *567*, 126–135. https://doi.org/https://doi.org/10.1016/j.jcis.2020.01.087.

(69) Qin, X.; Li, H.; Xie, S.; Li, K.; Jiang, T.; Ma, X.-Y.; Jiang, K.; Zhang, Q.; Terasaki, O.; Wu, Z.; et al. Mechanistic Analysis-Guided Pd-Based Catalysts for Efficient Hydrogen Production from Formic Acid Dehydrogenation. *ACS Catal.* **2020**, *10* (6), 3921–3932. https://doi.org/10.1021/acscatal.0c00225.

(70) Sun, Q.; Wang, N.; Xu, Q.; Yu, J. Nanopore-Supported Metal Nanocatalysts for Efficient Hydrogen Generation from Liquid-Phase Chemical Hydrogen Storage Materials. *Adv. Mater.* **2020**, 2001818. https://doi.org/10.1002/adma.202001818.

(71) Doustkhah, E.; Hasani, M.; Ide, Y.; Assadi, M. H. N. Pd Nanoalloys for H2 Generation from Formic Acid. *ACS Appl. Nano Mater.* **2020**, *3* (1), 22–43. https://doi.org/10.1021/acsanm.9b02004.

(72) Liu, D.; Gao, Z. Y.; Wang, X. C.; Zeng, J.; Li, Y. M. DFT Study of Hydrogen Production from Formic Acid Decomposition on Pd-Au Alloy Nanoclusters. *Appl. Surf. Sci.* **2017**, *426*, 194–205. https://doi.org/10.1016/j.apsusc.2017.07.165.

(73) Loza, K.; Heggen, M.; Epple, M. Synthesis, Structure, Properties, and Applications of

Bimetallic Nanoparticles of Noble Metals. *Adv. Funct. Mater.* **2020**, *30* (21), 1909260. https://doi.org/10.1002/adfm.201909260.

(74) Liu, X.; Astruc, D. From Galvanic to Anti-Galvanic Synthesis of Bimetallic Nanoparticles and Applications in Catalysis, Sensing, and Materials Science. *Adv. Mater.* **2017**, *29* (16), 1605305. https://doi.org/10.1002/adma.201605305.

(75) Zhu, Q. L.; Tsumori, N.; Xu, Q. Sodium Hydroxide-Assisted Growth of Uniform Pd Nanoparticles on Nanoporous Carbon MSC-30 for Efficient and Complete Dehydrogenation of Formic Acid under Ambient Conditions. *Chem. Sci.* **2014**, *5* (1), 195–199. https://doi.org/10.1039/c3sc52448e.

(76) Li, Z.; Yang, X.; Tsumori, N.; Liu, Z.; Himeda, Y.; Autrey, T.; Xu, Q. Tandem Nitrogen Functionalization of Porous Carbon: Toward Immobilizing Highly Active Palladium Nanoclusters for Dehydrogenation of Formic Acid. *ACS Catal.* **2017**, *7* (4), 2720–2724. https://doi.org/10.1021/acscatal.7b00053.

(77) Bi, Q.-Y.; Lin, J.-D.; Liu, Y.-M.; He, H.-Y.; Huang, F.-Q.; Cao, Y. Dehydrogenation of Formic Acid at Room Temperature: Boosting Palladium Nanoparticle Efficiency by Coupling with Pyridinic-Nitrogen-Doped Carbon. *Angew. Chemie - Int. Ed.* **2016**, *55*, 1–6.

(78) Cai, Y.; Li, X.; Zhang, Y.; Wei, X.; Wang, K.; Chen, J. Highly Efficient Dehydrogenation of Formic Acid over a Palladium- Angewandte. *Angew. Chemie - Int. Ed.* **2013**, *52* (45), 1–5. https://doi.org/10.1002/anie.201304652.

(79) Zhu, Q. L.; Tsumori, N.; Xu, Q. Immobilizing Extremely Catalytically Active Palladium Nanoparticles to Carbon Nanospheres: A Weakly-Capping Growth Approach. *J. Am. Chem.*

Soc. **2015**, *137* (36), 11743–11748. https://doi.org/10.1021/jacs.5b06707.

(80) Zhu, D.-J.; Wen, Y.-H.; Xu, Q.; Zhu, Q.-L.; Wu, X.-T. Surface-Amine-Implanting Approach for Catalyst Functionalization: Prominently Enhancing Catalytic Hydrogen Generation from Formic Acid. *Eur. J. Inorg. Chem.* **2017**, *2017* (40), 4808–4813. https://doi.org/10.1002/ejic.201701108.

(81) Sun, J.; Qiu, H.; Cao, W.; Fu, H.; Wan, H.; Xu, Z.; Zheng, S. Ultrafine Pd Particles Embedded in Nitrogen-Enriched Mesoporous Carbon for Efficient H2 Production from Formic Acid Decomposition. *ACS Sustain. Chem. Eng.* **2019**, *7* (2), 1963–1972. https://doi.org/10.1021/acssuschemeng.8b04130.

(82) Wang, X.; Meng, Q.; Gao, L.; Liu, J.; Ge, J.; Liu, C.; Xing, W. Metal Organic Framework Derived Nitrogen-Doped Carbon Anchored Palladium Nanoparticles for Ambient Temperature Formic Acid Decomposition. *Int. J. Hydrogen Energy* **2019**, *44* (53), 28402–28408. https://doi.org/10.1016/j.ijhydene.2019.05.083.

(83) Chen, Y.; Li, X.; Wei, Z.; Mao, S.; Deng, J.; Cao, Y.; Wang, Y. Efficient Synthesis of Ultrafine Pd Nanoparticles on an Activated N-Doping Carbon for the Decomposition of Formic Acid. *Catal. Commun.* **2018**, *108*, 55–58. https://doi.org/10.1016/j.catcom.2018.01.028.

(84) Wang, Q.; Tsumori, N.; Kitta, M.; Xu, Q. Fast Dehydrogenation of Formic Acid over Palladium Nanoparticles Immobilized in Nitrogen-Doped Hierarchically Porous Carbon. *ACS Catal.* **2018**, *8* (12), 12041–12045. https://doi.org/10.1021/acscatal.8b03444.

(85) Li, J.; Chen, W.; Zhao, H.; Zheng, X.; Wu, L.; Pan, H.; Zhu, J.; Chen, Y.; Lu, J. Size-

Dependent Catalytic Activity over Carbon-Supported Palladium Nanoparticles in Dehydrogenation of Formic Acid. *J. Catal.* **2017**, *352*, 371–381. https://doi.org/10.1016/j.jcat.2017.06.007.

(86) Ding, T. Y.; Zhao, Z. G.; Ran, M. F.; Yang, Y. Y. Superior Activity of Pd Nanoparticles Confined in Carbon Nanotubes for Hydrogen Production from Formic Acid Decomposition at Ambient Temperature. *J. Colloid Interface Sci.* **2019**. https://doi.org/10.1016/j.jcis.2018.12.017.

(87) Lee, J. H.; Ryu, J.; Kim, J. Y.; Nam, S.-W.; Han, J. H.; Lim, T.-H.; Gautam, S.; Chae, K. H.; Yoon, C. W. Carbon Dioxide Mediated, Reversible Chemical Hydrogen Storage Using a Pd Nanocatalyst Supported on Mesoporous Graphitic Carbon Nitride. *J. Mater. Chem. A* **2014**, *2* (25), 9490–9495. https://doi.org/10.1039/C4TA01133C.

(88) Doustkhah, E.; Rostamnia, S.; Zeynizadeh, B.; Kim, J.; Yamauchi, Y.; Ide, Y. Efficient H2 Generation Using Thiourea-Based Periodic Mesoporous Organosilica with Pd Nanoparticles. *Chem. Lett.* **2018**, *47* (9), 1243–1245. https://doi.org/10.1246/cl.180537.

(89) Koh, K.; Seo, J.-E.; Lee, J. H.; Goswami, A.; Yoon, C. W.; Asefa, T. Ultrasmall Palladium Nanoparticles Supported on Amine-Functionalized SBA-15 Efficiently Catalyze Hydrogen Evolution from Formic Acid. *J. Mater. Chem. A* **2014**, *2* (48), 20444–20449. https://doi.org/10.1039/c4ta04538f.

(90) Martis, M.; Mori, K.; Fujiwara, K.; Ahn, W. S.; Yamashita, H. Amine-Functionalized MIL-125 with Imbedded Palladium Nanoparticles as an Efficient Catalyst for Dehydrogenation of Formic Acid at Ambient Temperature. *J. Phys. Chem. C* **2013**, *117* (44), 22805–22810.

https://doi.org/10.1021/jp4069027.

(91) Zhong, H.; Su, Y.; Cui, C.; Zhou, F.; Li, X.; Wang, R. Palladium Nanoparticles Supported by Carboxylate-Functionalized Porous Organic Polymers for Additive-Free Hydrogen Generation from Formic Acid. *ACS Sustain. Chem. Eng.* **2017**, *5* (9), 8061–8069. https://doi.org/10.1021/acssuschemeng.7b01675.

(92) Xu, L.; Yao, F.; Luo, J.; Wan, C.; Ye, M.; Cui, P.; An, Y. Facile Synthesis of Amine-Functionalized SBA-15-Supported Bimetallic Au-Pd Nanoparticles as an Efficient Catalyst for Hydrogen Generation from Formic Acid. *RSC Adv.* **2017**, *7* (8), 4746–4752. https://doi.org/10.1039/C6RA26793A.

(93) Zhang, X.; Shang, N.; Shang, H.; Du, T.; Zhou, X.; Feng, C.; Gao, S.; Wang, C.; Wang, Z. Nitrogen-Decorated Porous Carbon Supported AgPd Nanoparticles for Boosting Hydrogen Generation from Formic Acid. *Energy Technol.* **2019**, *7*, 140–145. https://doi.org/10.1002/ente.201800522.

(94) Zhao, P.; Xu, W.; Yang, D.; Luo, W.; Cheng, G. Metal-Organic Framework Immobilized CoAuPd Nanoparticles with High Content of Non-Precious Metal for Highly Efficient Hydrogen Generation from Formic Acid. *ChemistrySelect* **2016**, *1* (7), 1400–1404. https://doi.org/10.1002/slct.201600397.

(95) Guo, X. T.; Zhang, J.; Chi, J. C.; Li, Z. H.; Liu, Y. C.; Liu, X. R.; Zhang, S. Y. Efficient Dehydrogenation of a Formic Acid-Ammonium Formate Mixture over Au 3 Pd 1 Catalyst. *RSC Adv.* **2019**, *9* (11), 5995–6002. https://doi.org/10.1039/c8ra09534e.

(96) Xu, L.; Jin, B.; Zhang, J.; Cheng, D.-G.; Chen, F.; An, Y.; Cui, P.; Wan, C. Efficient

Hydrogen Generation from Formic Acid Using AgPd Nanoparticles Immobilized on Carbon Nitride-Functionalized SBA-15. *RSC Adv.* **2016**, *6* (52), 46908–46914. https://doi.org/10.1039/c6ra06071d.

(97) Sun, Q.; Wang, N.; Bing, Q.; Si, R.; Liu, J.; Bai, R.; Zhang, P.; Jia, M.; Yu, J. Subnanometric Hybrid Pd-M(OH)2, M = Ni, Co, Clusters in Zeolites as Highly Efficient Nanocatalysts for Hydrogen Generation. *Chem* **2017**, *3* (3), 477–493. https://doi.org/10.1016/j.chempr.2017.07.001.

(98) Queiroz, L. S.; de Souza, L. K. C.; Thomaz, K. T. C.; Leite Lima, E. T.; da Rocha Filho, G. N.; do Nascimento, L. A. S.; de Oliveira Pires, L. H.; Faial, K. do C. F.; da Costa, C. E. F. Activated Carbon Obtained from Amazonian Biomass Tailings (Acai Seed): Modification, Characterization, and Use for Removal of Metal Ions from Water. *J. Environ. Manage.* **2020**, *270*, 110868. https://doi.org/10.1016/j.jenvman.2020.110868.

(99) Tang, Z. E.; Lim, S.; Pang, Y. L.; Shuit, S. H.; Ong, H. C. Utilisation of Biomass Wastes Based Activated Carbon Supported Heterogeneous Acid Catalyst for Biodiesel Production. *Renew. Energy* **2020**, *158*, 91–102. https://doi.org/10.1016/j.renene.2020.05.119.

(100) Osman, A. I.; Farrell, C.; Al-Muhtaseb, A. H.; Harrison, J.; Rooney, D. W. The Production and Application of Carbon Nanomaterials from High Alkali Silicate Herbaceous Biomass. *Sci. Rep.* **2020**, *10* (1), 1–13. https://doi.org/10.1038/s41598-020-59481-7.

(101) Yang, V.; Arumugam Senthil, R.; Pan, J.; Rajesh Kumar, T.; Sun, Y.; Liu, X. Hierarchical Porous Carbon Derived from Jujube Fruits as Sustainable and Ultrahigh Capacitance Material for Advanced Supercapacitors. *J. Colloid Interface Sci.* **2020**, *579*, 347–356.

https://doi.org/10.1016/j.jcis.2020.06.080.

(102) Jain, D.; Kanungo, J.; Tripathi, S. K. Enhancement in Performance of Supercapacitor Using Eucalyptus Leaves Derived Activated Carbon Electrode with CH_3COONa and HQ Electrolytes: A Step towards Environment Benign Supercapacitor. *J. Alloys Compd.* **2020**, *832*, 154956. https://doi.org/10.1016/j.jallcom.2020.154956.

(103) Titirici, M.-M.; White, R. J.; Falco, C.; Sevilla, M. Black Perspectives for a Green Future: Hydrothermal Carbons for Environment Protection and Energy Storage. *Energy Environ. Sci.* **2012**, *5* (5), 6796–6822. https://doi.org/10.1039/C2EE21166A.

(104) Titirici, M. M.; Antonietti, M. Chemistry and Materials Options of Sustainable Carbon Materials Made by Hydrothermal Carbonization. *Chem. Soc. Rev.* **2010**, *39* (1), 103–116. https://doi.org/10.1039/b819318p.

(105) Lillo-Ródenas, M. A.; Lozano-Castelló, D.; Cazorla-Amorós, D.; Linares-Solano, A. Preparation of Activated Carbons from Spanish Anthracite - II. Activation by NaOH. *Carbon.* **2001**, *39* (5), 751–759.

(106) Linares-Solano, A.; Lozano-Castelló, D.; Lillo-Ródenas, M. A.; Cazorla-Amorós, D. Carbon Activation by Alkaline Hydroxides Preparation and Reactions, Porosity and Performance. *Chemistry and Physics of Carbon*. 2008, pp 1–62.

(107) Maciá-Agulló, J. A.; Moore, B. C.; Cazorla-Amorós, D.; Linares-Solano, A. Activation of Coal Tar Pitch Carbon Fibres: Physical Activation vs. Chemical Activation. *Carbon.* **2004**, *42* (7), 1367–1370. https://doi.org/10.1016/j.carbon.2004.01.013.

(108) Wang, H.; Zhou, Y.; Zhao, Q.; Zhang, X.; Di, L. NH3 Plasma Synthesis of N-Doped Activated Carbon Supported Pd Catalysts with High Catalytic Activity and Stability for HCOOH Dehydrogenation. *Int. J. Hydrogen Energy* **2020**, No. xxxx. https://doi.org/10.1016/j.ijhydene.2020.05.209.

(109) Gödde, J.; Merko, M.; Xia, W.; Muhler, M. Nickel Nanoparticles Supported on Nitrogen–Doped Carbon Nanotubes Are a Highly Active, Selective and Stable CO_2 Methanation Catalyst. *J. Energy Chem.* **2021**, *54*, 323–331. https://doi.org/10.1016/j.jechem.2020.06.007.

(110) Luo, W.; Wang, B.; Heron, C. G.; Allen, M. J.; Morre, J.; Maier, C. S.; Stickle, W. F.; Ji, X. Pyrolysis of Cellulose under Ammonia Leads to Nitrogen-Doped Nanoporous Carbon Generated through Methane Formation. *Nano Lett.* **2014**, *14* (4), 2225–2229.

(111) Inagaki, M.; Toyoda, M.; Soneda, Y.; Morishita, T. Nitrogen-Doped Carbon Materials. *Carbon.* **2018**, *132*, 104–140. https://doi.org/10.1016/j.carbon.2018.02.024.

(112) Salinas-Torres, D.; Navlani-García, M.; Mori, K.; Kuwahara, Y.; Yamashita, H. Nitrogen-Doped Carbon Materials as a Promising Platform toward the Efficient Catalysis for Hydrogen Generation. *Appl. Catal. A Gen.* **2019**, *571*, 25–41. https://doi.org/10.1016/J.APCATA.2018.11.034.

(113) Caiti, M.; Padovan, D.; Hammond, C. Continuous Production of Hydrogen from Formic Acid Decomposition Over Heterogeneous Nanoparticle Catalysts: From Batch to Continuous Flow. *ACS Catal.* **2019**, *9* (10), 9188–9198. https://doi.org/10.1021/acscatal.9b01977.

For Table of Contents Use Only

TOC

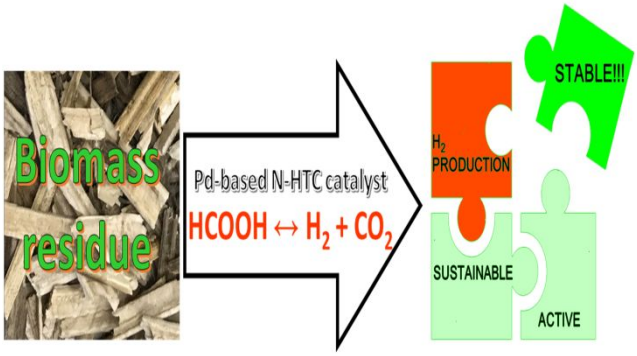

SYNOPSIS. Highly active and stable catalysts from biomass upgrading were designed as a platform for the sustainable hydrogen production from formic acid.